Study of Amides and Organic Acids over the North-West Indo-Gangetic Plain in the Monsoon Season

Hiral Gandhi
MS16072

A dissertation submitted for the partial fulfillment of the BS-MS Dual Degree in Science

Indian Institute of Science Education and Research, Mohali

April, 2021

Certificate of Examination

This is to certify that the dissertation titled "**Study of Amides and Organic Acids over the North-West Indo-Gangetic Plain in the Monsoon Season**" submitted by **Ms. Hiral Gandhi** (MS16072) for the partial fulfilment of BS-MS dual degree program of the Institute, has been examined by the thesis committee duly appointed by the Institute. The committee finds the work done by the candidate satisfactory and recommends that the report be accepted.

Dr. V. Sinha (Supervisor)

Dr. R. Attada

Dr. A.Ambili

Dated: April 30, 2021

Declaration

The work presented in this dissertation has been carried out by me under the guidance of Dr. Vinayak Sinha at the Indian Institute of Science Education and Research, Mohali.
This work has not been submitted in part or in full for a degree, a diploma, or a fellowship to any other university or institute. Whenever contributions of others are involved, every effort is made to indicate this clearly, with due acknowledgement of collaborative research and discussions. This thesis is a bonafide record of original work done by me and all sources listed within have been detailed in the bibliography.

Hiral Gandhi
(Candidate)

Dated: April 30, 2021

In my capacity as the supervisor of the candidate's project work, I certify that the above statements by the candidate are true to the best of my knowledge.

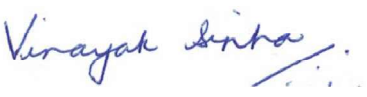

Dr. V. Sinha
(Supervisor)

Acknowledgment

I would like to express my gratitude to Dr. Vinayak Sinha, my project supervisor for his kind supervision and guidance in completing my dissertation. I am indebted for his continuous patient guidance, support, enthusiasm, feedback and suggestions, which motivated me to learn more and work harder towards the project. I am thankful to the committee members Dr. Raju Attada and Dr.Anoop Ambili for providing their valuable inputs. I acknowledge Dr. Sachin Ghude, Dr. Kaushar Ali and Prodip Acharya of IITM Pune for valuable inputs on pH of rainwater and aerosol.

I would also like to thank IISER Mohali for providing a conducive environment which was very helpful for completing the thesis in time. I acknowledge the Ministry of Human Resource Development and DST - INSPIRE Scholarship for support and funding.

On a personal note I would like to thank my friends at IISER Mohali and outside for helping throughout a very difficult past year. I would like to thank Saksham for being my strongest pillar of support and motivation, and being there for me throughout the best and the worst times. I would like to thank Sparsh for motivating and inspiring me to work hard during times I felt stuck. I would like to thank Gaurav for never letting me doubt myself and being a wonderful friend. I would like to thank Kimaya and Cheshta for being the best of friends from the very beginning of college and for all the fun times we had together.

I would also like to thank my lab mates - Haseeb bhaiya, Ashish bhaiya , Shabin bhaiya, Vidit bhaiya, Raj, Saurabh and Pooja di and others for helping me throughout the course of my thesis.

List of Figures

List of Tables

Notation (Abbreviations)

1. **NW-IGP:** North-West Indo-Gangetic Plain
2. **VOC:** Volatile organic compounds
3. **PTR-MS:** Proton transfer reaction mass spectrometer
4. **PA :** Proton Affinity
5. **SEM :** Secondary Electron Multiplier
6. **ICA :** Isocyanic Acid
7. **RH :** Relative Humidity
8. **BLH :** Boundary Layer Height

Contents

Abstract

Isocyanic acid, a potentially harmful organic acid, was measured in the ambient air a decade ago. While its primary sources include biomass burning and traffic emissions, it is formed photochemically from amides reacting with the hydroxyl (OH) radical. This study aims at further investigating the production of isocyanic acid from these precursor compounds and look into the possible sinks during the monsoon season at a suburban site in the NW-IGP.

The VOCs were measured using an online Proton Transfer Reaction – Mass Spectrometer and the data for the period 06-07-2019 to 08-08-2019 (n>12000 measurements) at a 4-minute temporal resolution was analyzed in this study. The average VOC concentrations during this period were 0.86 ppb, 5.4 ppb, 0.65 ppb, 0.23 ppb, 0.13 ppb for isocyanic acid, formamide, acetamide, Sum of C3 Amides and Sum of C4 amides respectively.

Diel profiles of isocyanic acid and the amides showed a daytime peak indicating a strong photochemical source. Average daytime peak of isocyanic acid reached ~1 ppb which is believed to be a concern as it might pose health risks. Sources and sinks were investigated by calculating the rates of formation of isocyanic acid. The calculated rate of formation (32.99 x 10^{-6} ppb/sec) was found to be ~ 3 times the observed rate of formation (10.7x10^{-6} ppb/sec) from 6:00am to 13:00 pm. This is because observed rate of formation comprises of both sources and sinks while calculated rate of formation doesn't account for the sinks. By comparing this value with the observed rate of isocyanic acid formation and applying mass balance the sink was determined to be 22.29 x 10^{-6} ppb/sec. Our results suggest deposition could be a major sink of isocyanic acid during the monsoon season over north-west IGP.

Chapter 1

Introduction

1.1 Isocyanic Acid: Overview and Health Risks

Isocyanic acid (HNCO) has been known since 1830, when it was shown to be formed on the depolymerization of Cyanuric Acid[1]. However, it was only recently measured in ambient air and emissions from biomass burning at concentrations that could potentially pose a health risk[2]. This is because isocyanic acid is highly soluble at physiological pH, and isocyanic acid and its aqueous cyanate ion (NCO^-) is has been identified as an intermediate in the protein carbamylation reactions [3]. It has been found in multiple studies that protein carbamylation and its corresponding inflammatory response leads to adverse health issues like cataracts, cardiovascular problems and even chronic disorders like rheumatoid arthritis [3–5]. Also its structure is similar to methyl isocyanate (CH_3NCO), which is a highly toxic compound as was found during its accidental leak from a pesticide plant in Bhopal, India, causing deaths and diseases in thousands of people [6].

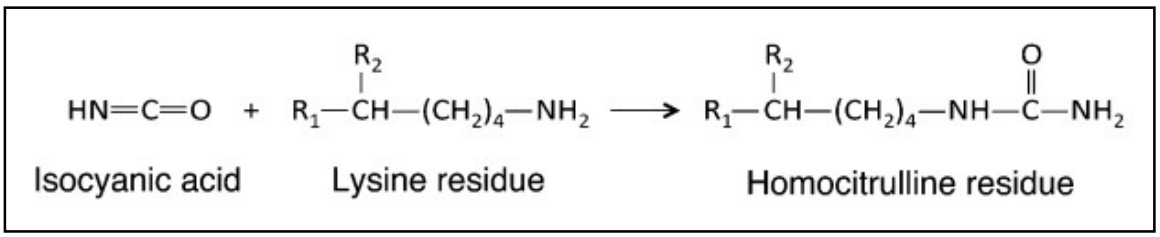

Figure 1.1 An example of a carbamylation reaction by isocyanic acid. (Source: Gorisse, L. et al 2015 [7])

In the study by Roberts et al 2011[2], they calculated the Henry's Law Constant of HNCO at pH=3and used that to estimate that HNCO would be highly soluble at physiological pH=7.4 with the Henry's Law solubility value of 10^5 M/atm. It was calculated from this solubility that inhalation of ambient air having isocyanic acid concentrations greater than 1ppb can result in formation of high enough equilibrium concentration of NCO^-(100μM) which is known to mimic carbamylation in vitro [3].

However in a very recent article [8], it was shown that these conclusions might not be very true. A healthy individual had, on an average, a concentration of 45nM of isocyanic acid in their blood plasma. Even in people suffering from chronic renal failure had HNCO and urea concentrations 141nM and 28mM respectively [9]. The values of measured concentrations from the Roberts et al study were more than thousand times the values associated with severe chronic conditions and thus could be very significant. This contrast in values is because the concentration from Roberts et al. 2011 (100 μM) was calculated by assuming the solubility and reactivity in a pure water system. Even on assuming that the body has no elimination mechanisms, it would take a person 600 days to build up such a high dose of 100 μM in the blood plasma, and the bodily elimination systems might also be playing a significant role which cannot be ruled out [8]. Hence it becomes even more important to accurately quantify its concentration and study its sources and sinks to accurately predict its health risks.

1.2 Isocyanic Acid: Sources

Many places across the world have now recorded isocyanic acid in ambient air as can be seen in Table 1. In India, it was first recorded in ambient air by Chandra et al. 2016[10], at a site in the North-West Indo-Gangetic Plain. This study shows a clear secondary photochemical production as a source of isocyanic acid along with primary emissions from biomass burnings. This is similar to methyl isocyanate (CH_3NCO) which is also formed as a major product from the photochemical oxidation of methyl isocyanide (CH_3NC) by OH radicals[11] apart from its primary emission sources.

Apart from this many other sources of isocyanic acid have been identified like from cigarette smoke [12], gasoline and diesel vehicles[13–16] and extractions from oil sands [17].

Location	Reagent ion/MS	Avg. Mixing Ratio (ppbv)	Reference
Mohali, India	H3O+/quad	0.940 (mean)	Chandra et al. 2016[10]
Kathmandu Valley, Nepal	H3O+/ToF	0.900 (mean)	Sarkar et al. 2016[18]
Toronto, Ontario	Acetate/ToF	Fall: 0.100 (mean), 0.080	Hems et al. 2019[12]

		(median)	
	Acetate/quad	Summer: 0.085 (mean)	Wentzell et al. 2013[13]
	Iodide/ToF	Summer: 0.045 (mean), 0.039 (median) Winter: 0.025 (mean), 0.015 (median)	Wren et al. 2018[16]
La Jolla, California	Acetate/quad	0.081 (mean)	Zhao et al. 2014[19]
Erie, Colorado	Acetate/quad	Winter: 0.072 (mean), 0.065 (median)	Roberts et al. 2014[20]
	Acetate/ToF	Summer: 0.030 (mean)	Mattila et al. 2018[21]
Fort Collins, Colorado	Acetate/quad	0.055 (mean), 0.050 (median)	Roberts et al. 2014[20]
Calgary, Alberta	Acetate & iodide/quad	0.036 (mean), 0.034 (median) Winter: 0.028 (mean), 0.033 (median)	Woodward-Massey et al. 2014[22]
Pasadena, California	Acetate/quad	Summer: 0.025 (mean), 0.022 (median)	Roberts et al. 2011, 2014[2,20]
Canadian Arctic Archipelago	Acetate/ToF	0.020 (mean), 0.016 (median)	Mungall et al. 2017[23]
Manchester, UK	Iodide/ToF	0.012 (mean)	Priestley et al. 2018[24]
Guangzhou , Pearl River Delta, China (urban)	ToF-CIMS	Fall: 0.46 (mean)	Wang Z et al. 2020[25]
North China Plain, China (rural)	ToF-CIMS	Winter: 0.37 (mean)	Wang Z et al. 2020[25]

Table 1. Average HNCO concentrations measured in ambient air from different locations across the world. (Modified from the table obtained from Leslie et al, 2019[26])

In the laboratory biomass burning experiment by Roberts et al. (2011), the emission time profile of the fire was measured and it was found that HNCO emissions were higher during the flaming stage while the HNCO concentrations were lower in the smoldering stage. The HNCO concentration was also highly correlated with the CO concentrations during the flaming stage of the fire and this ratio could be used to identify biomass burning events. This data was then compared to the ambient measurements from the FourMile Canyon Wildfire in Boulder, Colorado in 2010 and ambient data from LA. While the concentrations in laboratory experiment went as high as 600ppbv, the ambient background concentration of HNCO was about 10pptv and went to about 200pptv during the FourMile fire and up to 100pptv at the LA site. The high concentrations in the lab experiments could also be because the burning smoke was measured very close to the source. The FourMile fire was consistent with the smoldering stage concentrations of HNCO and CO from the lab experiment fire. This shows that biomass burning is an important source of HNCO emissions in the atmosphere. Apart from this they observed a clear diurnal variation in the HNCO concentration at the LA site (Figure 1.2) in a period when there were no wildfires, hence eliminating wildfires as a source of HNCO. This suggests that HNCO is formed photochemically from precursor compounds like amines and amides.

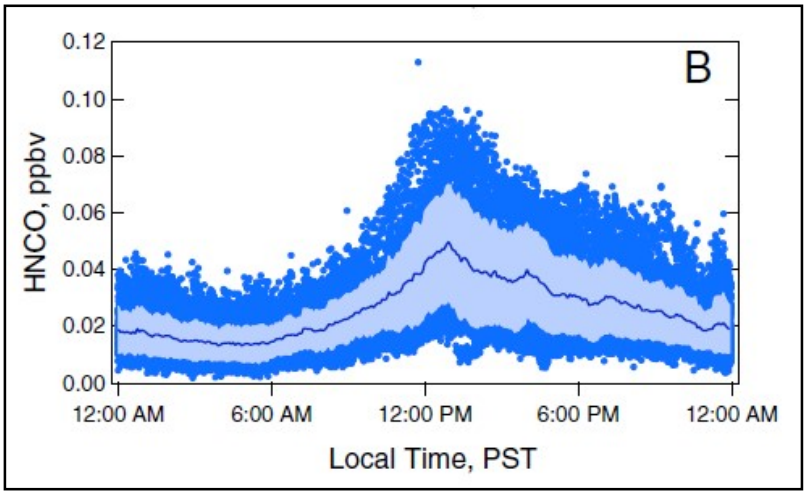

Figure 1.2.1 Diurnal variation of HNCO at the LA site – 20 second measurements(blue dots), 5 min average concentrations (blue line) and ±1σ (light blue shaded region) (Source: Roberts et al. 2011)

Many precursor compounds have now been identified which lead to secondary photochemical formation of isocyanic acid like urea [27], nicotine [28], amines [29] and amides [30]. So basically the amines get oxidized to amides which in turn get oxidized to isocyanates [31].

A very recent study (Wang Z et al. 2020) [25] done at a field campaign in China tried to find the sources and precursor compounds of isocyanic acid. The urban site(Pearl River Delta) recorded an average of 0.46ppbv of HNCO while the rural site(North China Plain) recorded an average of 0.37ppbv. These measurements were about 10 times higher than those measured in LA[2] and Canada[22].What was observed was that while the urban site had a clear diurnal variation with an afternoon peak indicating secondary photochemical formation, the rural site had comparatively stable concentrations throughout the day with a morning peak indicating that there was both primary emission and secondary formation at the rural site. Next they tried to identify the precursor compounds of HNCO by calculating the rates of secondary formation of HNCO using the measured concentrations of formamide and C_2-C_{10} amides, since amides have already been identified as precursors of HNCO. It was found that C_3 amide concentrations were the largest among amides and it contributed to 74% of the HNCO production in the extreme case calculation (Figure 1.2.2 (a)). The concentrations (hourly average) of HNCO went up to 1ppbv while that of C_3 amide went up to 5.6ppbv (Figure1.2.2 (b)). Also it was observed that C_3 amides had higher concentrations at night in contrast to the HNCO peak during the daytime (Figure 1.2.2 (c)). Also a correlation plot of C_3 amide vs. styrene, which is a marker for industrial emissions, was made and a good correlation was observed indicating that the C_3 amides were emitted from industrial emissions (Figure1.2.2 (d)).

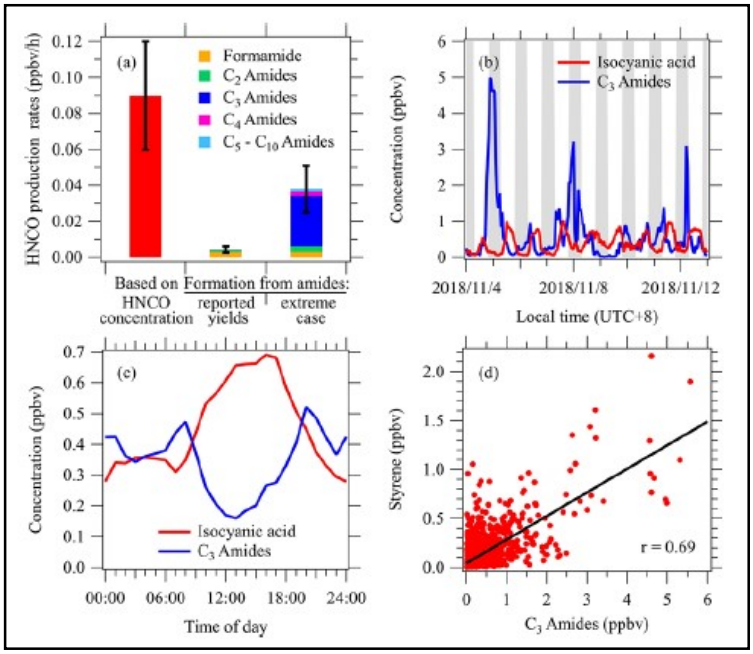

Figure 1.2.2 All plots are from measurements from the urban (PRD) site. (a)Comparison of HNCO production rates from steady state analysis and calculated contributions from various amides. Reported yields: the production rate calculated from the reported yields of amides. Extreme Case: production rate calculated assuming all the nitrogen of the amides is converted to HNCO (100% yield) (b) Time series of HNCO and C_3 amides at the urban site during the campaign period. (c) Diurnal variation of HNCO and C_3 amides. (d) Correlation plot of C3 amides with styrene. ("Reprinted with permission from - High Concentrations of Atmospheric Isocyanic Acid (HNCO) Produced from Secondary Sources in China, Zelong Wang, Bin Yuan, Chenshuo Ye, James Roberts, Armin Wisthaler, Yi Lin, Tiange Li, Caihong Wu, Yuwen Peng, Chaomin Wang, Sihang Wang, Suxia Yang, Baolin Wang, Jipeng Qi, Chen Wang, Wei Song, Weiwei Hu, Xinming Wang, Wanyun Xu, Nan Ma, Ye Kuang, Jiangchuan Tao, Zhanyi Zhang, Hang Su, Yafang Cheng, Xuemei Wang, and Min Shao, *Environmental Science & Technology* 2020 *54* (19), 11818-11826, DOI: 10.1021/acs.est.0c02843. Copyright 2020 American Chemical Society.")

From these results it was concluded that secondary formation was the major source of HNCO in Guangzhou, China and might validate the claim by Link et al., 2016[32] that photochemical

formation might be a more important source of HNCO than primary emissions in urban areas. Also while amides might be precursors of HNCO, the production rate of HNCO from amides was significantly lower than the total production rate required to maintain the corresponding concentrations thus hinting that there might be other precursors for which further studies might be required.

1.3 Isocyanic Acid: Loss Processes

On extrapolating the already available data for isocyanic acid at high temperatures, the rate constant for reactivity with OH radicals to be 1.24 x 10^{-15} cm^3 $molecule^{-1}$ s^{-1} corresponding to an atmospheric lifetime of HNCO as long as several decades [33]. Hence this shows that removal of isocyanic acid from the atmosphere via gas phase reactions is a slow process. Also isocyanic acid is stable against photolysis from the solar radiation [34] and its lifetime with respect to the same is calculated to be in the order of a few months[2]. Hence the main loss processes of isocyanic acid in the atmosphere comprise of wet and dry deposition [35].

The lifetime of isocyanic acid with respect to hydrolysis is highly dependent on the temperature, water content in the air and the pH of the cloud droplets. The gas to liquid partitioning is governed by the Henry's Law constant $K_{H,}$ which for isocyanic acid is highly dependent on the pH of water and was calculated to be 26±2 M atm^{-1}. Once it is dissolved, it can undergo three different reactions depending on the pH of the solution as shown in the Figure 1.3 [35]. Another study estimated the aqueous fraction of HNCO and found that it could better estimate the HNCO scavenged by cloud water than predicted by the Henry's law coefficient thus confirming the importance of aqueous phase partitioning in determining the lifetime of HNCO in the atmosphere.[19]

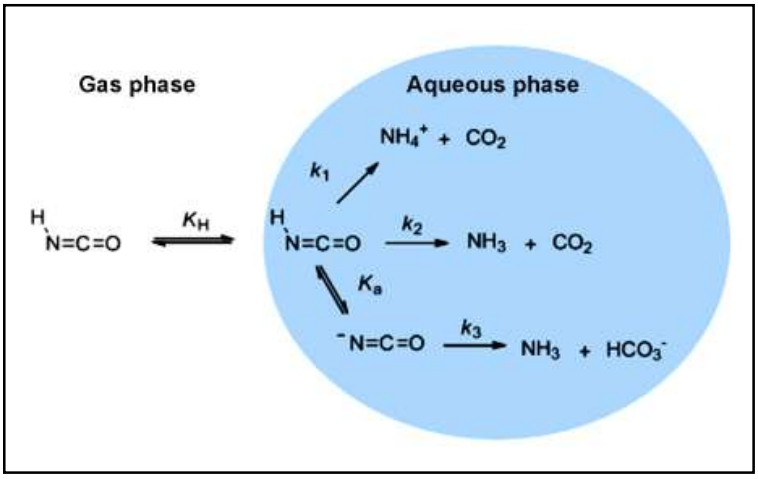

Figure 1.3 Possible hydrolysis mechanisms for isocyanic acid (Source: Borduas et al 2016[35], License link)

A recent study in the Pearl River Delta in China (an urban site) observed rapid dry deposition from the diurnal profiles and calculated the atmospheric lifetime isocyanic acid against dry deposition to range between 6-16 hours[25].

Recently Roberts et al., 2019[36], also reported the lifetime of isocyanic acid against such heterogeneous processes. This was calculated using the Henry's law coefficient at different pH to calculate the uptake coefficient γ_{rxn} using the formula:

$$\gamma_{rxn} = \frac{4H_{eff}RT\sqrt{kD_a}}{<c>} \qquad \text{-------- Eq. 1}$$

Here, H_{eff} is the Henry's law coefficient, R is the gas constant, T is the temperature, D_a is the diffusion coefficient, k is the first order loss rate and <c> is the mean molecular speed. Once this is calculated, it is used to calculate the deposition velocity V_d using the formula:

$$\nu_d \cong \gamma \frac{<c>}{4} \qquad \text{-------- Eq. 2}$$

Once the V_d was obtained, it was used to get the lifetime since lifetime is given by h/ V_d where h is the PBL height. The atmospheric lifetime of isocyanic acid with respect to dry

deposition to neutral pH surfaces in the boundary layer was calculated to be about 1 day and 6-12 days with respect to aerosol deposition.

This hence seems to be an important sink in contrast to photolysis and gas phase photochemistry. These conclusions were also confirmed in a recent study where the results from the atmospheric EMAC model also predicted that the gas phase chemical loss contributes to less than 1% of loss processes, cloud precipitation contributes to around 10% of removal of HNCO and dry deposition contributes to about 90% loss globally, thus being a major sink for HNCO[37].

1.4 Isocyanic Acid: Chemical Transport Modelling

A study by Young et al., 2012[38], used the MOZART-4 chemical transport model to estimate the global concentrations of HNCO and to identify areas where the concentrations of HNCO might be higher based on their environmental conditions. The model included primary emissions from biomass burnings and other anthropogenic sources and loss processes including reaction with OH radical, dry and wet deposition which is pH dependent. Hence the Henry's law coefficient H_{eff} was also calculated using the model calculated pH and the simulation run using this value was the control simulation (called pH_calc). Simulations were also run using parameters if the pH was 2 everywhere and similarly from pH 3-7 to compare the effect of pH on the HNCO abundance and its tropospheric budget. In the simulation run using the H_{eff} from model calculated pH, the highest annual average surface HNCO concentration were measured over China of approximate 470 pptv as can be seen in Figure 1.4.1.

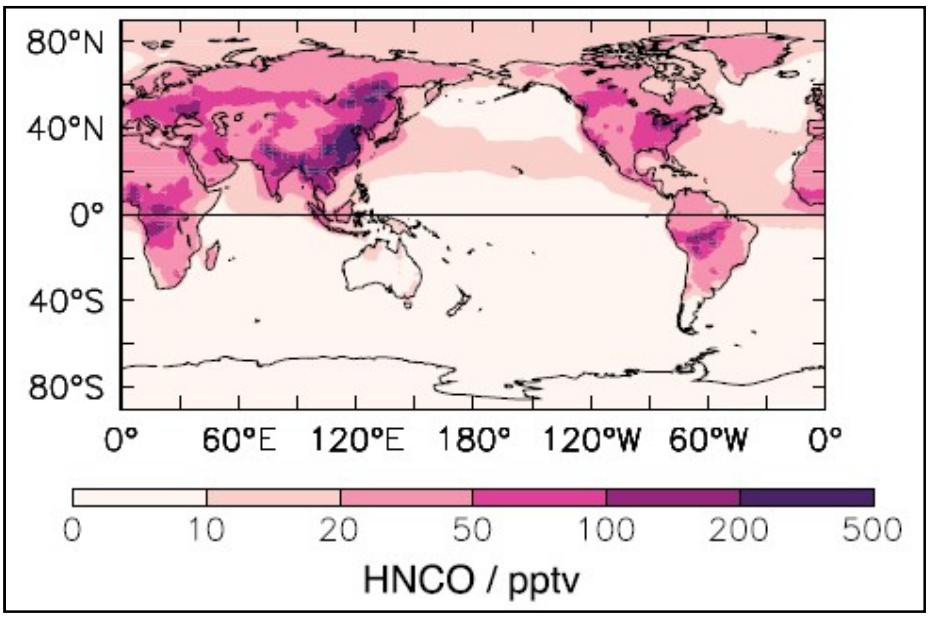

Figure 1.4.1 Annual mean surface concentrations of HNCO obtained from the control simulation. (Source: Young et al., 2012[38] , License Number:5040191114711)

It was found that the regions having high primary emissions from biomass burning like South-East Asia, tropical Africa, Siberia, Canada and the Amazon had the highest concentrations of HNCO which often exceeded the 1ppbv limit. Hence the model also calculated the number of days for which the HNCO concentrations exceeded 1ppbv in these different regions and how many people did that affect in each respective region. It was found that while Siberia exceeded 1ppbv limit for the maximum number of days, since South-East Asia is densely populated, the highest number of people exposed to it were in the South-East Asian region (Figure 1.4.2).

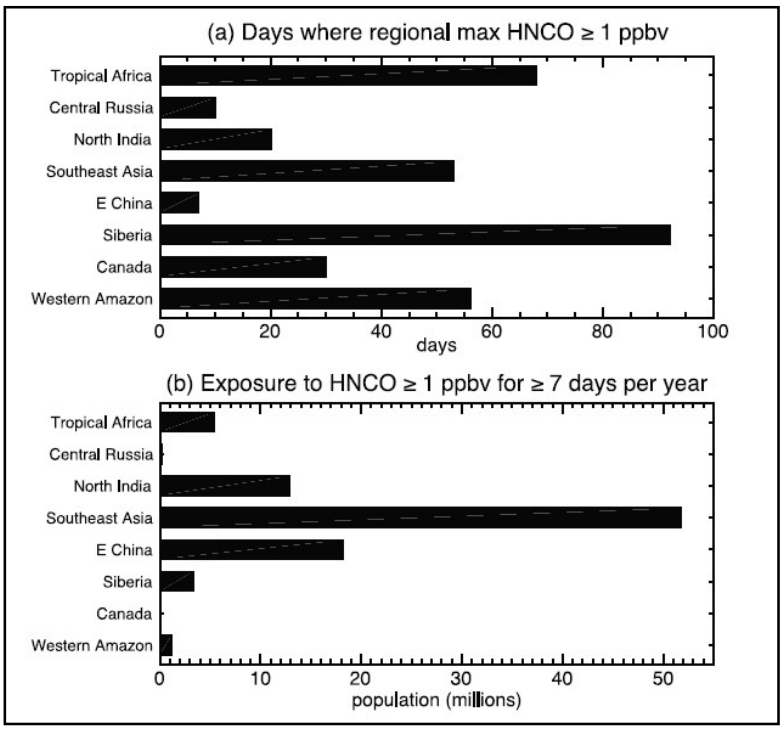

Figure 1.4.2 (a) Number of days where HNCO concentrations exceeded 1ppbv. (b)Number of people exposed to HNCO greater than 1ppbv for more than 7 days a year.(Source: Young et al., 2012 , License Number: 5040191114711)

Apart from this, the global tropospheric budget was also calculated for different pH simulations. The importance of the pH of the cloud droplets was demonstrated in these simulations since it controlled the percentage of loss via wet deposition and it can be seen that wet deposition becomes the dominant loss process on increasing the pH (Figure 1.4.3 (b)). It was also observed that the burden and the lifetime decreased on increasing the pH and hence indicating that the model calculated pH must be lower (2-4) (Figure 1.4.3(a) and (c)). This was likely due to the absence of basic influence of Ca^{2+} from the soil dust. Hence this indicates that pH is highly important when estimating the transport of HNCO from the emitting areas to remote areas since it controls the atmospheric lifetime and loss rates. It was found that HNCO export was greatly reduced in the high pH (6-7) simulations.

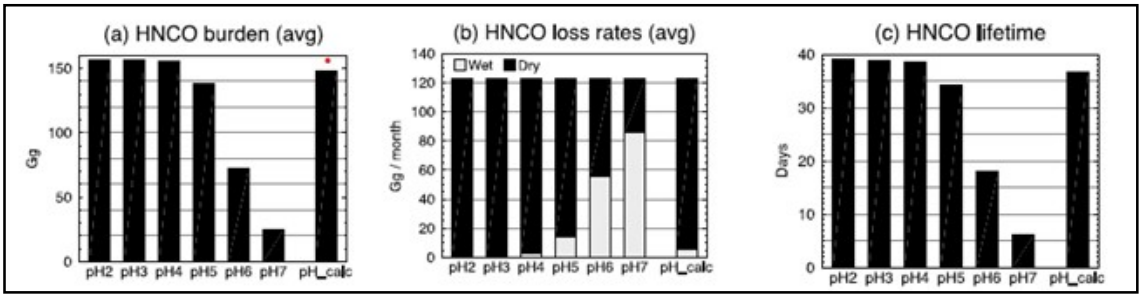

Figure 1.4.3 Plots for simulations pH 2-7 and control simulation (pH_calc) (a) Average tropospheric burden for the year at different pH simulations (Gigagrams of HNCO) (b) Monthly loss rates of HNCO via both wet and dry deposition at different pH simulations (c) tropospheric lifetime of HNCO at different pH simulations (Source:Young et al., 2012 , License Number: 5040191114711)

However this model was run with some limitations and incomplete understanding of the sources and sinks of HNCO and hence more observational data and research is required to get better model estimations. However one conclusion that stands is that regions with high primary emissions from biomass burnings and other anthropogenic emissions are exposing their populations to higher concentrations of HNCO which could potentially be a health risk. Also further studies are required to know exactly what concentrations of HNCO could cause what health effects for better risk assessment at different regions in the world.

Chapter 2

Materials and Methods

2.1 Site Description

All the measurements of Isocyanic acid concentrations and ambient air pollutants like CO_2, PM2.5, NO_x were recorded from the Atmospheric Chemistry and Emissions Laboratory at the Indian Institute of Science Education and Research, Mohali, India. It is located in the city of Mohali, in a suburban region, 310 meters above mean sea level (30.667° N − 76.729° E). The area is located in the North-West Indo-Gangetic Plane (NW-IGP), South-West of the Tricity Area comprised of the three cities- Mohali, Chandigarh and Panchkula and close to the foothills of Himalayan Mountain Range as seen below in Figure 2.1.

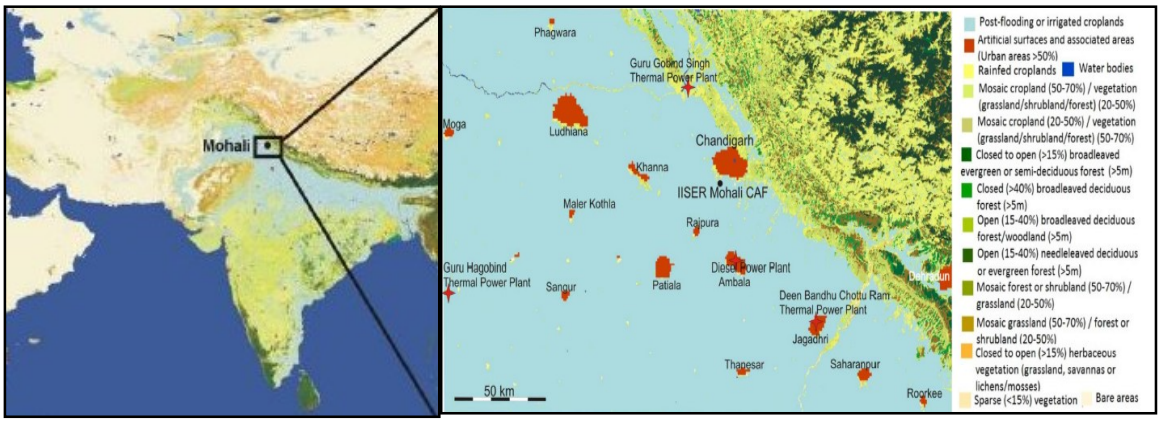

Figure 2.1 Left- Map marking the location of Mohali; Right- Map describing the land use of the area of 100 km × 200 km surrounding the measurement site (black dot – 30.667^0 N, 76.729^0 E) (Source: Sinha et al 2014[39], License link)

The institute campus is residential with tree cover throughout. As discussed above, the North West to North to East sector comprises of the tricity area and hence is classified an urban sector. A few small-scale industrial units are located surrounding the campus in the South to East sector like paint, pharmaceutical and solvent industries, glass manufacturing units and

brick kilns. The National Highways 1 and 2 also lie in this sector, which connect the city to the national capital New Delhi which is about 300kms South of the site. The South to North-West Sector is mostly agricultural land. Further site description, land use and land cover details, and sampling techniques are described in Sinha et al 2014[39].

2.2 Criteria for selecting the time period under study and prevalent meteorological conditions

The PTR-MS records Isocyanic Acid at *m/z* ratio 44. The supporting data used in this study also involves the data recorded by the PTR-MS at *m/z* 46, 60, 74 and 88 which are predicted to be formamide, acetamide, C3 amides and C4 amides – which are the predicted precursor compounds in the secondary formation of isocyanic acid. The data analyzed in this study was for the period of monsoon 2019 from 06-07-2019 to 08-08-2019. Before choosing this time period the data for the entire year was cleaned and corrected and the diel profiles were plotted. The annual average concentration of Isocyanic Acid was 0.84 ppb. The seasons were split as Winter (01-01-2019 to 02-03-2019), Summer (03-03-2019 to 04-07-2019), Monsoon (04-07-2019 to 04-10-2019) and Post Monsoon (05-10-2019 to 03-12-2019). The Figure 2.2.1(a) and (b) below show the diel profile of Isocyanic Acid concentration for the year 2019 and the season-wise diel profile respectively.

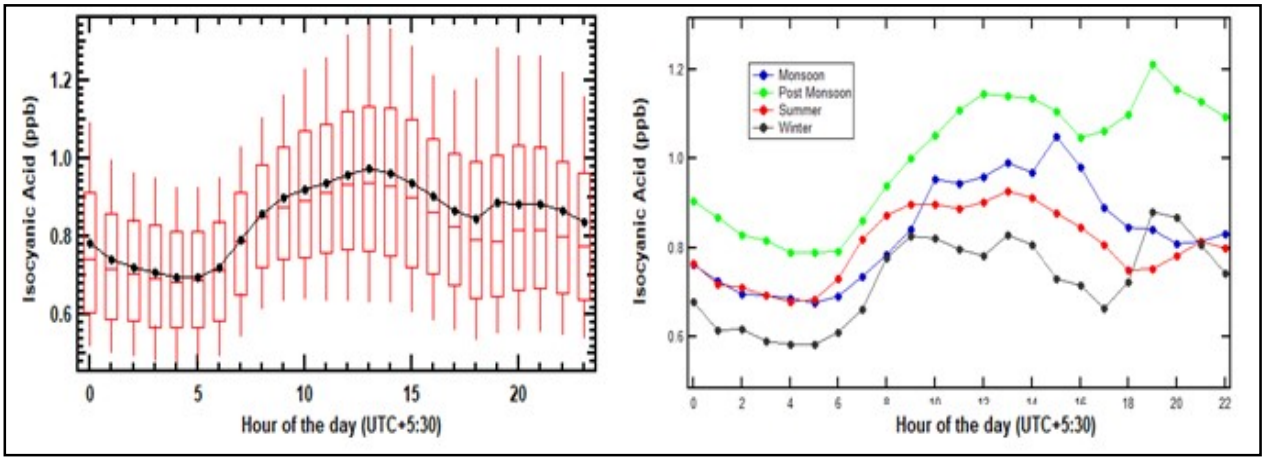

Figure 2.2.1 (a) Diel profile for Isocyanic acid concentrations for the year 2019 (b) Season-wise average diel profile for Isocyanic acid for the year 2019

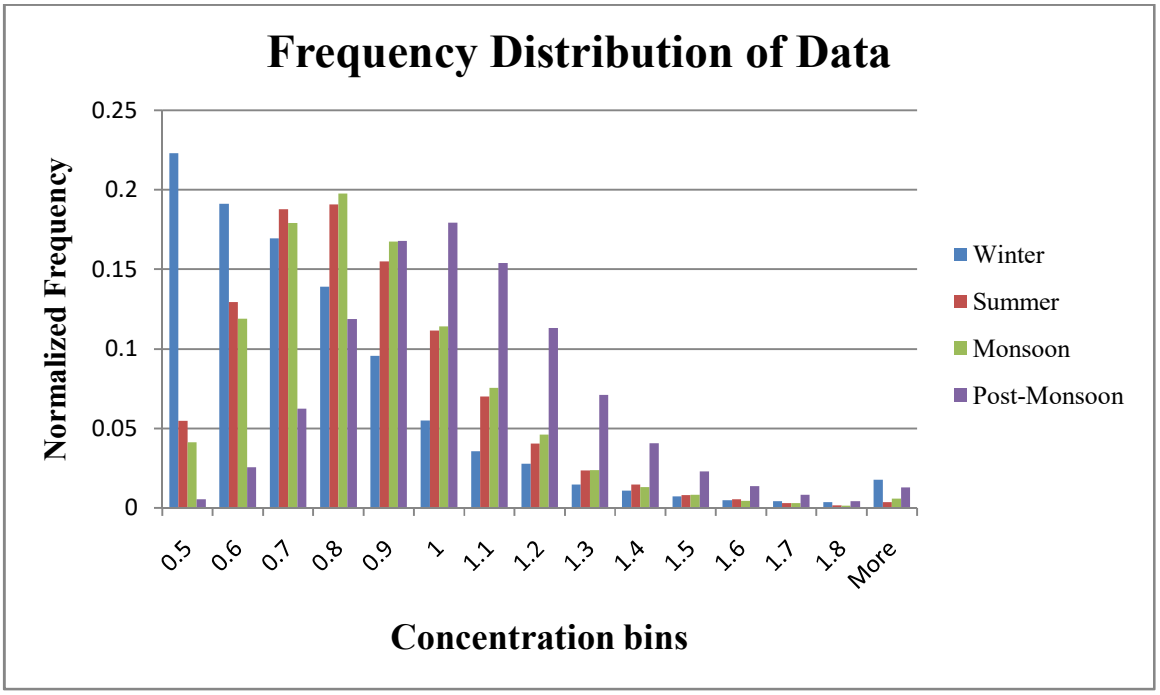

Figure 2.2.2 Normalized frequency distribution of data points for different seasons for 2019 (y-axis denotes normalized frequency and x-axis denotes the upper limit of concentration for each specific bin).

Isocyanic Acid shows a daytime peak which is due to strong photochemical production during the daytime. The nighttime peak is due to primary emission sources like traffic emissions or biomass burnings, etc. The post-monsoon has the highest average concentration with a night-time peak which is consistent with the emissions from biomass burning which is prevalent in the region during the post-monsoon season. A detailed study on the contribution of this biomass burning in post-monsoon on ambient isocyanic acid concentrations can be found in Chandra et al, 2016[10]. It was observed from the plots above that monsoon had higher average daytime concentrations as compared to summer which was against the expected behavior. Also monsoon had slightly higher frequencies of data points at higher concentrations (>0.7ppb) as compared to summer. Summer is expected to have higher daytime concentrations due to greater secondary photochemical production being expected as monsoon has more overcast days which reduce the solar radiation and hence lower photochemical formation. This further motivated to analyze the monsoon period. A calendar plot was made for the year 2019 to check for availability of data to choose the period, as can be seen in

Figure2.2.3 below. Finally the data from monsoon period 06-07-2019 to 08-08-2019 was chosen for further analysis.

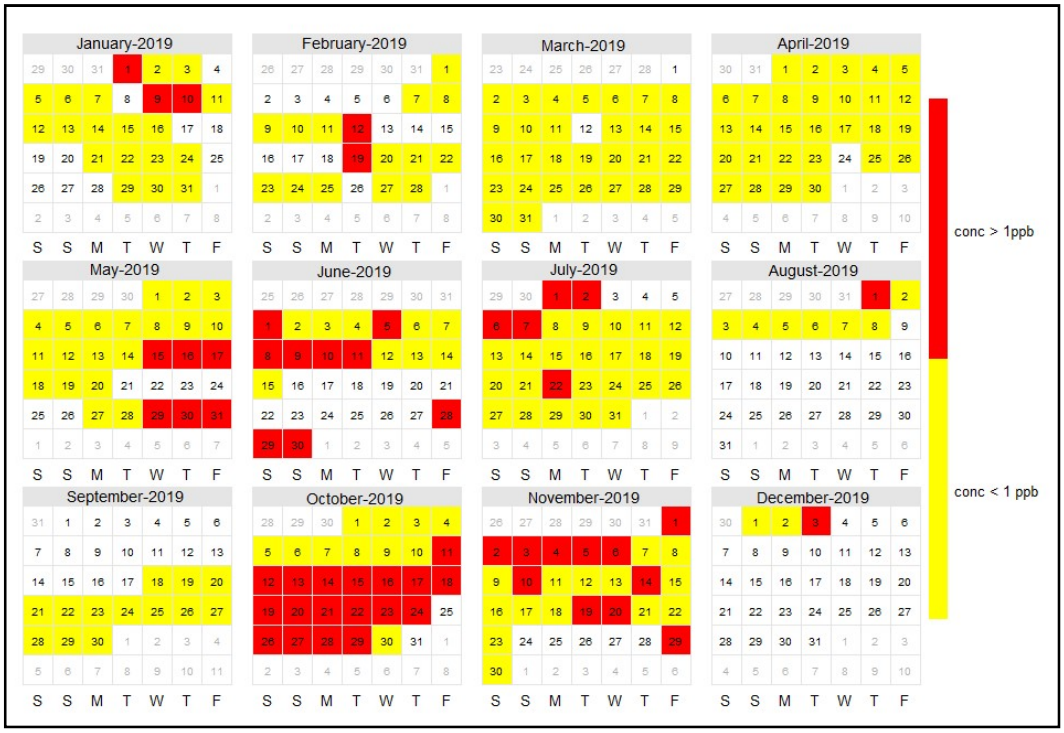

Figure 2.2.3 Calendar plot for Isocyanic Acid concentrations for the year 2019. Yellow denotes days with daily average concentration less than 1ppb while Red denotes days with daily average concentration greater than 1 ppb

Meteorological parameters like Wind Speed, Wind Direction, Ambient Temperature, Relative Humidity, and Solar Radiation were measured using the Meteorological Station installed on site (Met One Instruments Inc., Rowlett, Texas, USA).

The Figure 2.2.5 shows the diel profiles of ambient temperature, relative humidity, solar radiation and wind speed during the period of study. The average ambient temperature for the period was 28.9ºC with the minimum and maximum recorded temperature during the period being 21.5ºC and 37.8ºC respectively. The average humidity during the period was ~71% and the average daytime solar radiation peaked at ~435 W/m^2 at 13:00hrs. The lower solar radiation is because the period under study is associated with the Indian Summer Monsoon season with frequent episodes of rainfall and overcast skies.

The Figure 2.2.4 represents the wind rose plot for the period under study. As can be seen, the predominant fetch region is South East which is consistent with the Indian Summer Monsoon Season and the average wind speeds during the period were ~1.8 m/s.

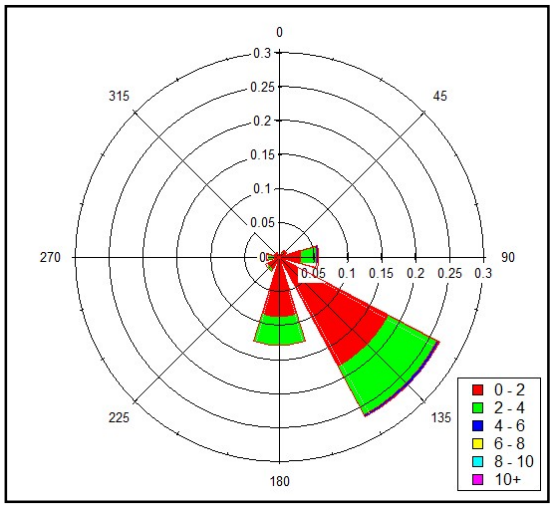

Figure 2.2.4 Wind Rose plot for the period 06-07-2019 to 08-08-2019, obtained from on-site wind speed and wind direction data. The radius axis represents the probability for an air mass to arrive from that particular direction and speed bin.

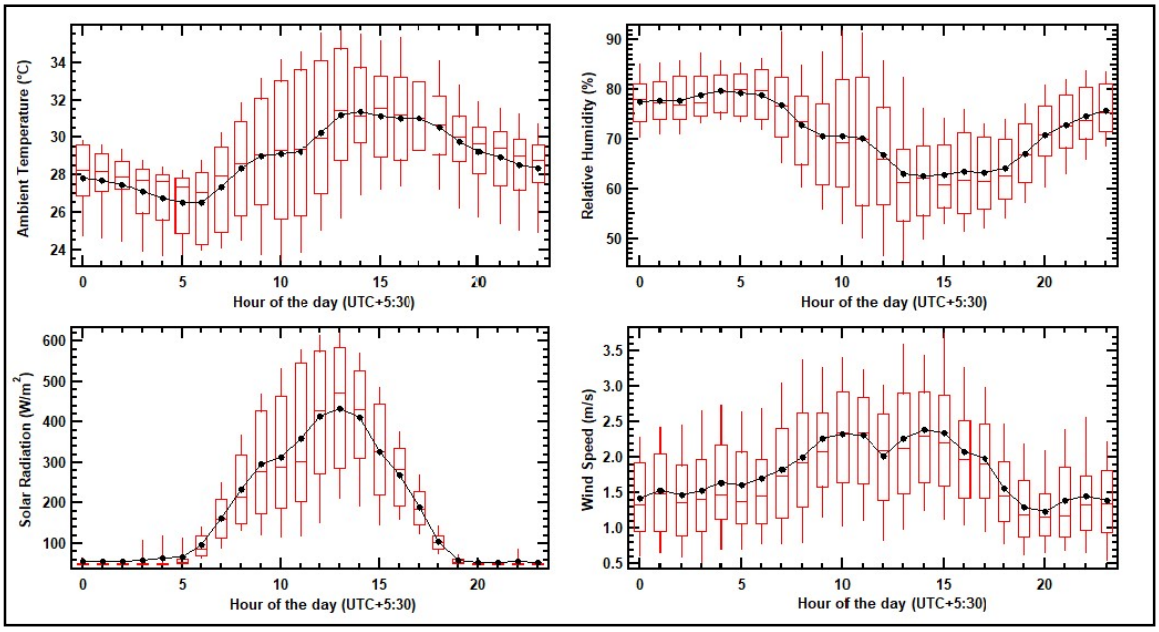

Figure 2.2.5 Diel profile for on-site prevalent meteorological conditions during the period of study 06-07-2019 to 08-08-2019 - (a) Ambient Temperature, (b) Relative Humidity, (c) Solar Radiation, (d) Wind Speed.

2.3 VOCs measured using a Proton Transfer Reaction – Mass Spectrometer (PTR-MS)

The concentrations of all the volatile organic compounds reported in this thesis were measured using an on-site Proton Transfer Reaction-Quadrupole Mass Spectrometer (PTR-QMS) manufactured by Ionicon. (HS Model 11-07HS-088; Ionicon Analytik Gesellschaft, Austria).

The PTR-MS was built by Professor Werner Lindinger and his group in 1998 at the University of Innsbruck, Austria[40]. The technique works on the chemical ionization principle which is a soft ionization technique- meaning that is produces negligible or no fragmentation of the ions. The analyte molecules undergo a proton transfer from the reagent ions (H_3O^+) which are then detected by a quadrupole mass spectrometer. Since water has a proton affinity (P.A.) = 165.2 Kcal/mol, only the molecules with greater P.A than this undergo ionization and hence only such molecules can be detected. It is a highly sensitive instrument and can measure, in real time, trace quantities of Volatile Organic Compounds upto a few pptv in concentration.

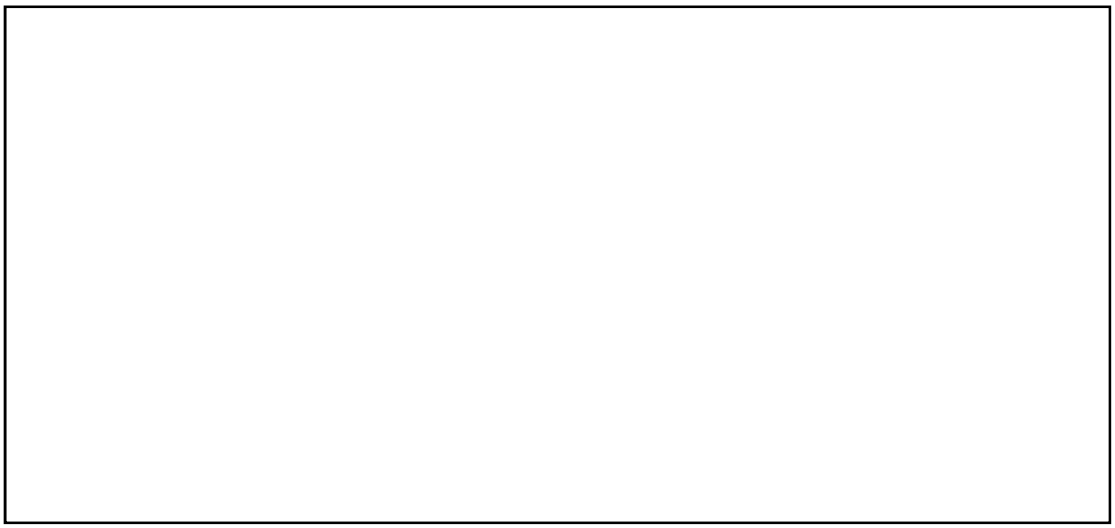

Figure 2.3 Schematic Diagram of the PTR-QMS Instrument (Source: de Gouw, J et al 2007[41] License Number: 5040210449872)

The Figure 2.3 above shows the diagram of the PTR-MS with its components in the order: Ion Source, Drift Tube, Quadrupole Mass Analyzer and Detector (Secondary Electron Multiplier). The following is the process involved in measuring the analytes:

1. Pure water is introduced through the inlet which is then converted to a pure stream of reagent H_3O^+ ions (>95%) using plasma discharge in a hollow cathode tube.
2. The H_3O^+ ions then enter the drift tube. The analyte molecules (R) are also introduced into the drift tube from the air inlet. The analyte molecules with P.A. greater than that of water are protonated by reacting with the H_3O^+ ions.

$$H_3O^+ + R \rightarrow RH^+ + H_2O \qquad \text{-------- Eq. 3}$$

3. The ions are separated based on their *m/z* ratio by the Quadrupole Mass Analyzer which allows ions with only one *m/z* ratio to pass through at a time.
4. They are then detected by the Secondary Electron Multiplier (SEM). The SEM amplifies the charges to produce a current which is then converted to the signal which is recorded in the computer.

This study also involved measurements for some other supporting parameters like CO, NO_x and PM2.5. The Table 2 below mentions the instruments used for measurement of each of the trace gases mentioned above and their working principle.

Instrument	Working principle	Target species
PM 2.5 Analyzer	β-Attenuation	PM 2.5
NO_x Analyzer	Chemiluminescence	NO and NO2
CO Analyzer	Non-dispersive Infrared Spectroscopy (NDIR)	CO

Table 2. List of analyzers used and the respective principles they work on

2.4 Data Quality Assurance - Calibration experiment

Calibration experiment was performed to determine the sensitivity and the detection limits of the VOCs. Instrument background was taken by passing the zero air which was generated by passing the zero air from cylinder (Sigma gases; 99.9999% purity) through a Gas Calibration

Unit (GCU-s v2.1; Ionimed Analytik, Innsbruck, Austria). Next the flow of calibration gas (Apel-riemer Environmental, Inc., Colorado, USA) dynamically diluted by a constant flow of zero air was introduced to the PTR-MS for the calibration. The ion signal obtained is of the unit counts per second (cps) which is then normalized with respect to hydronium ions(obtained by $H_3O(18)^+$ x 500) and hydronium ion water clusters to normalized counts per second (ncps) using the following formula obtained from Sinha et al, 2009[42] :

$$\text{ncps} = \frac{I(RH^+)\times 10^6}{(I(H_3O_{18}^+)\text{ x } 500)+I(H_3O^+)(H_2O)} \times \frac{2}{\text{P}_{\text{drift}}} \times \frac{\text{T}_{\text{drift}}}{273.18} \qquad \text{------ Eq. 4}$$

This obtained ncps was the measured response which was plotted against the introduced concentration (ppb) and the slope of this plot was the sensitivity factor for the compound in ncps/ppb. This sensitivity factor was the used to convert the ncps of each compound to concentration in ppb. The sensitivity factors can also be calculated theoretically using the equation derived from de Gouw and Warneke, 2007[41] as shown in Eq.5 below. It was found that the sensitivity factor obtained from the quadratic fit when compared to the one obtained theoretically, the uncertainty was less than 40%.

$$Sensitivity = \frac{k}{10^9} \text{ x } \frac{NA\,L^2}{22400 \text{ x } \mu_0 \text{ x } U_{drift}} \text{ x } \frac{{T_0}^2}{{T_{drift}}^2} \text{ x } \frac{{P_{drift}}^2}{{P_0}^2} \text{ x } \frac{T(RH^+)}{T(H_3O^+)} \qquad \text{----- Eq. 5}$$

Where:

k = rate coefficient for proton-transfer reaction

L = length of drift-tube (9.3 cm)

μ_0 = ion mobility of H_3O^+

N = number density of the gas in drift tube

T (RH^+) = transmission efficiency for RH^+

T (H_3O^+) = transmission efficiency for H_3O^+

P_0 = air pressure at STP

T_0 = temperature at STP

However the compounds in this study- measured at *m/z* 44,46,60,74 and 88 do not have an available gas standard for calibration and hence their sensitivity factors are obtained from the

quadratic fit of the curves obtained from the calibration experiment done on 29-06-2019 of the available VOCs. The graph for the same experiment can be seen below in Figure 2.4.1.

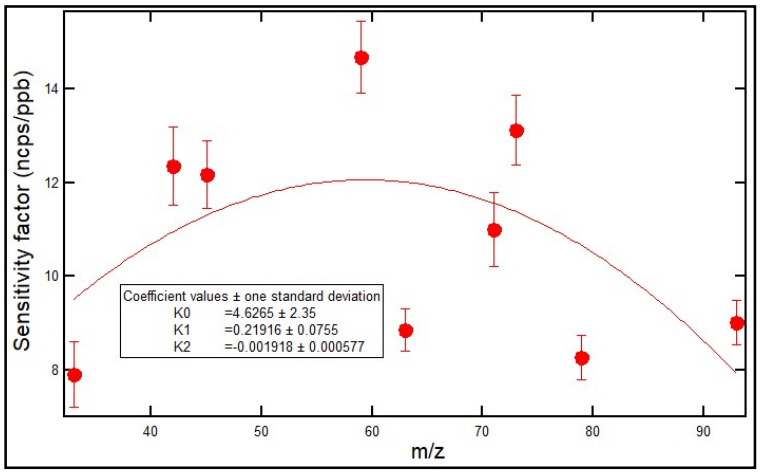

Figure 2.4 Calibration experiment done on 29-06-2019. The quadratic fit equation was used to calculate the sensitivity factors for the compounds used in this study. The vertical bars represent standard deviation of the sensitivity factors obtained from the calibration experiment.

m/z	ncps/ppb
44	10.394
46	10.472
60	10.57
74	9.884
88	8.414

Table 3. Sensitivity factors obtained from the quadratic fit for the compounds used in this study

The sensitivity factors obtained are summarized in Table 3 above. The sensitivity factors which were derived using calibration experiments and the ones theoretically derived for the compounds were within ~40% of each other. The sensitivity factors reported in some other studies for isocyanic acid were – 22.6 ncps/ppb in Borduas et al, 2015 [31] and 25.57 obtained from the quadratic fit in Warneke et al, 2011 [43]. The values for sensitivity factors obtained from our calibration experiment for acetonitrile (*m/z* 42) and acetaldehyde (*m/z* 45) were 12.36 and 12.18 respectively. The values for the same from Warneke et al, 2011 [43] were

25.39 and 25.65 respectively. Hence we can say that the systems were different and may have different parameters like transmission efficiency which caused this difference in sensitivity factors. This hence justifies the difference in the value of sensitivity factors calculated from the quadratic fit. Also the detection limit for isocyanic acid for the machine used in our study was less than 0.08 ppb as reported in Chandra et al, 2016[10].

Once the sensitivity factors were derived, the following steps were carried out to correct and clean the data:

1. The raw data (ncps) for each compound was converted to concentration by using the obtained sensitivity factor for that compound.
2. The data for the periods when the machine was showing alarms for internal parameters like P_{drift}, and cases when impurity ion concentrations exceeded the normal range was removed.
3. The data for the period when machine was used for other experiments (not measuring ambient air) was removed.

Chapter 3

Results and Discussion

3.1 General variability in time series of isocyanic Acid and precursor compounds

The mass assignments of compounds should be considered as upper limits for the mixing ratios as minor isobaric interferences cannot be ruled from compounds other than those attributed to at these mass channels. At m/z 46, the PTR-MS can detect dimethylamine, ethylamine and formamide but since dimethylamine and ethylamine are not formed photochemically, I have attributed daytime concentrations to be primarily formamide. Also, NO2+, which is an impurity ion is also measured at m/z 46 and hence m/z 46 will be considered strictly as an upper bound for formamide. A daytime correlation was done between m/z 46 and NO2 data, the correlation coefficient was found to be -0.4.
Similarly at m/z 60, the PTR-MS can detect trimethylamine ad acetamide but since trimethylamine is not formed photochemically, I have attributed daytime concentrations to acetamide primarily and m/z 60 will be considered as upper bound for acetamide.43 At m/z 74 and 88, multiple isomers for C3 and C4 amide compounds can be detected and hence m/z 74 and 88 will be considered as sum of C3 amides and sum of C4 amides respectively.
The figure 3.1 below shows the 1-minute average time series for the period of study for isocyanic acid (m/z 44), formamide(m/z 46), acetamide(m/z 60), sum of C3 amides(m/z 74) and sum of C4 amides(m/z 88).
Average concentrations for the period were observed as0.86 ppb, 5.4 ppb, 0.65 ppb, 0.23 ppb, 0.13 ppb for isocyanic acid, formamide, acetamide, Sum of C3 Amides and Sum of C4 amides respectively.

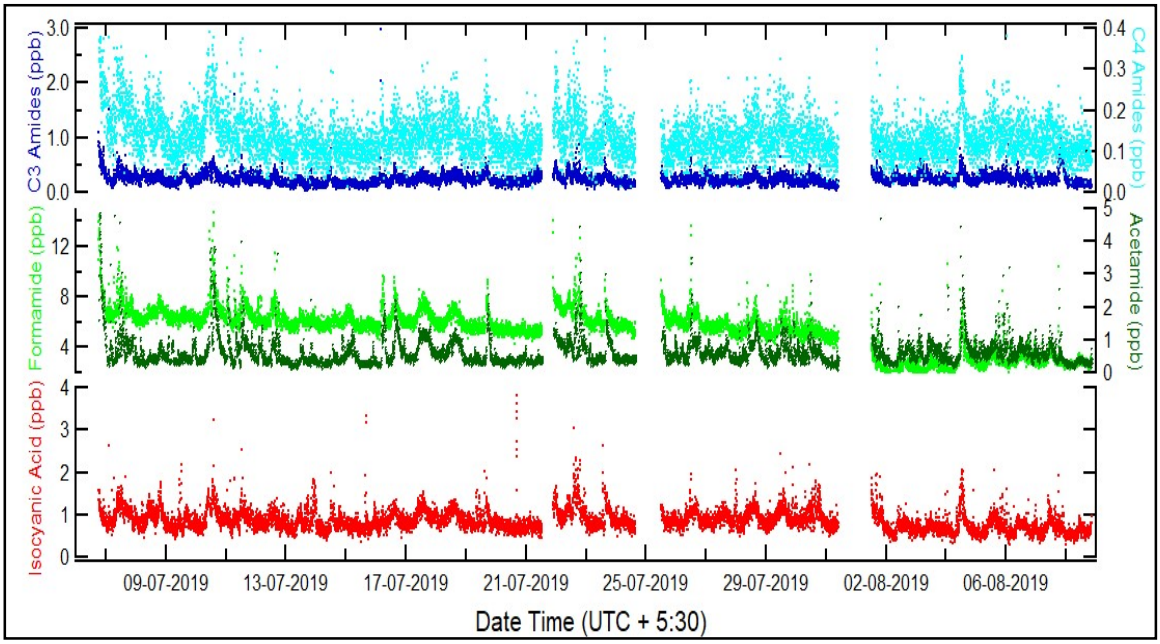

Figure 3.1 Time series plot of 4-minute temporal resolution for the mixing ratios of Isocyanic Acid (bottom panel), Formamide and Acetamide (middle panel), Sum of C3 and Sum of C4 Amides (top panel) for the period under study

3.2 Analysis of diel variability of isocyanic acid and precursor compounds in the monsoon season

In this analysis the diel profiles of isocyanic acid and precursor compounds were analyzed. The number of data points for isocyanic acid and precursor compounds were n>12000. The diel profile for isocyanic acid can be seen in Figure 3.2.1. Since isocyanic acid is photochemically formed, a daytime peak in concentrations is observed with the peak average concentration reaching ~1.00 ppb at 13:00 and 16:00 pm. This is agreement as the solar radiation peak of ~435 W/m^2 for the season also occurs at 13:00pm as can be seen in figure 2.2.4.

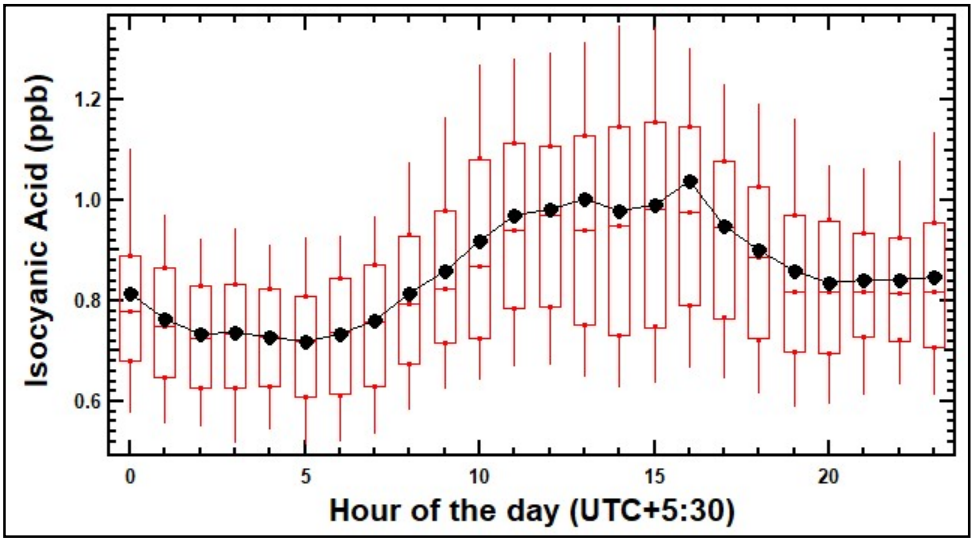

Figure 3.2.1 Diel profile for Isocyanic Acid concentrations

The diel profiles for the precursor compounds plotted for the period can be seen in Figure 3.2.2. Just like isocyanic acid, all the 4 precursors are also photochemically formed and have a similar diel profile where a daytime peak is observed. Table 4below lists the peak daytime concentrations of the precursor compounds.

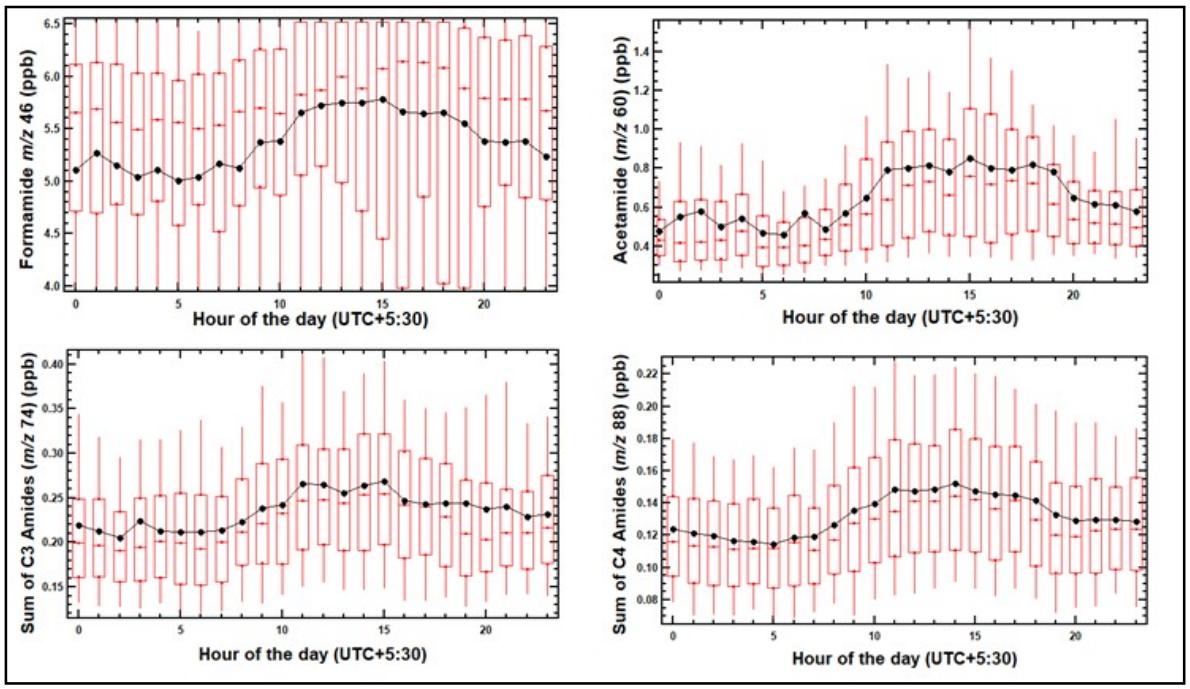

Figure 3.2.2 Diel profile for (a) Formamide (b) Acetamide (c) Sum of C3 Amides (d) Sum of C4 Amides

	Peak Concentration (ppb)	Peak time
Formamide	**5.8 ppb**	**15:00 pm**
Acetamide	**0.85 ppb**	**15:00 pm**
Sum of C3 Amides	**0.27 ppb**	**15:00 pm**
Sum of C4 Amides	**0.15 ppb**	**14:00 pm**

Table 4. Peak daytime concentrations of precursor compounds

Also, the diel profile for Carbon monoxide (CO) and NOx, tracers for combustion and traffic emissions, were plotted as can be seen in Figure 3.2.5 below. These compounds are not photochemically formed and hence do not show daytime peak.

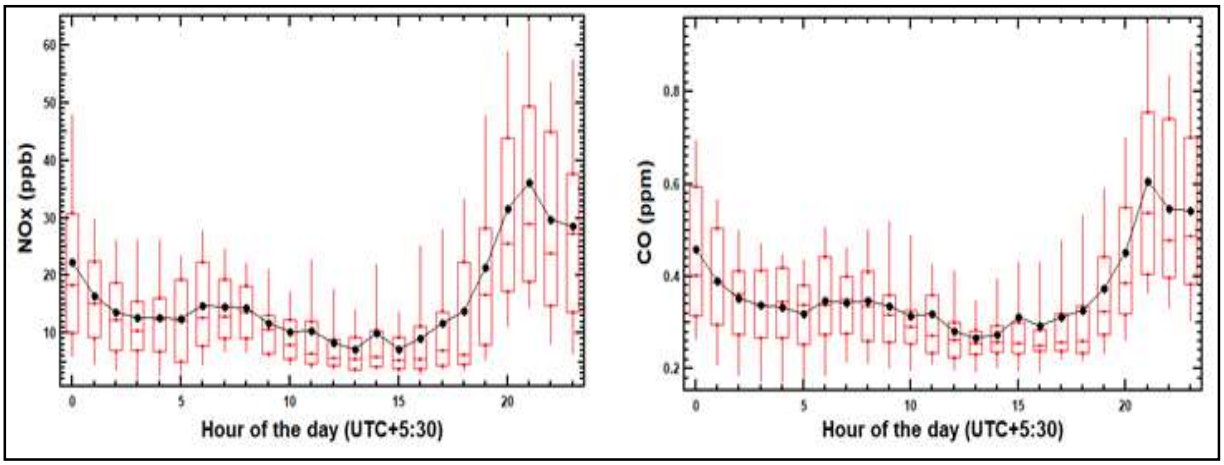

Figure 3.2.3 Diel profile for (a) NO_x (ppb) (b) CO(ppm)

Also, boundary layer height plays a very important role in the concentration on trace VOCs since greater the boundary layer height, greater the volume of air in which the gas is emitted and hence lower concentration. The Figure 3.2.4 below shows the diel plot of boundary layer height and ventilation coefficient.

$$\boldsymbol{Ventilation\ coefficient = Boundary\ layer\ height\ (m)\ \mathrm{x}\ Windspeed(m/s)} \quad \text{----- Eq. 6}$$

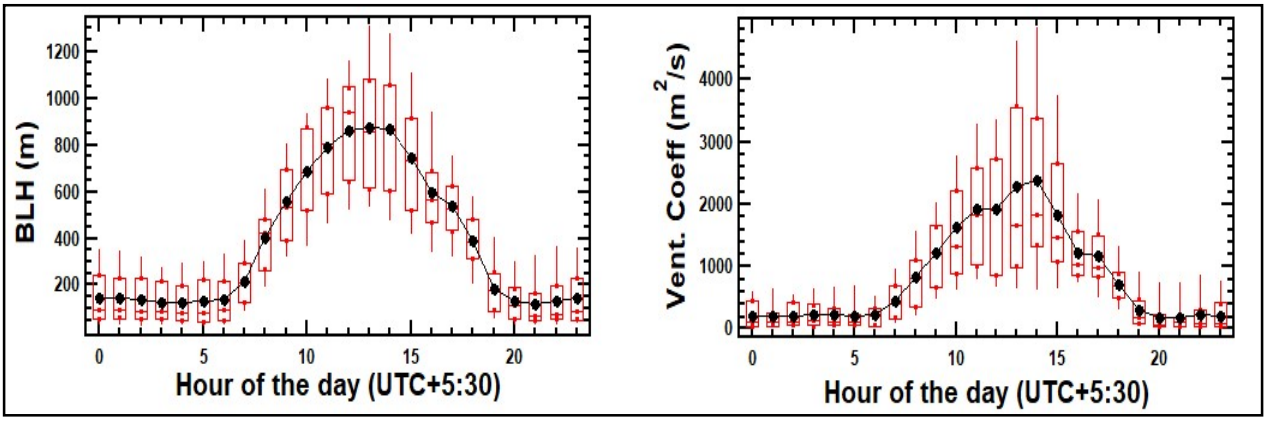

Figure 3.2.4 Diel profile for (a) BLH (m) (b) Ventilation Coefficient (m^2/s)

It can be seen that both BLH and ventilation coefficient have a daytime peak meaning that greater dilution takes during the daytime which could play a role in keeping the daytime concentrations of amides and isocyanic acid from going very high.

3.3 Calculation of photo-chemical production rate of isocyanic acid

Further analysis was done into the production and loss processes of Isocyanic Acid. The rate of formation of any species in the atmosphere is dependent on the net production and net loss processes. Also since during the daytime Isocyanic acid is mostly photochemically formed from the precursor compounds, the maximum rate of formation will be achieved during the daytime from sunrise to daytime solar radiation peak time. In the further sections, it will be discussed how the Observed and Calculated Rate of formation was obtained.

3.3.1. Observed rate of formation of isocyanic acid

The observed rate of formation was calculated by using the hourly average concentration of isocyanic acid from the diel plot in figure 3.2.1 from sunrise to the time of peak solar radiation which was obtained from the diel plot of solar radiation for the entire period of study in Figure 2.2.4 (c) as 6:00 am and 13:00 pm respectively. The rate of formation is then given as:

$$(R_{HNCO})_{observed} = \frac{\triangle HNCO}{\triangle t} \qquad \text{----- Eq. 7}$$

Where:

$\triangle$HNCO = average $HNCO_{[13:00]}$ – average $HNCO_{[06:00]}$

$\triangle t = 3600 \times 7 = 25200$ s

The observed rate of formation was calculated for the period as 10.7×10^{-6} ppb/sec. Note that observed rate of formation includes both sources and sinks and is hence expected to be lower than the calculated rate of formation.

3.3.2. Calculated rate of formation of isocyanic acid

Isocyanic acid is formed photochemically by reaction of precursor compounds with OH radical. The equations for these reactions are as follows:

- From Formamide : (Source: V Kumar et al,2018 [44])

  Pathway 1:

  $$HCONH_2 + \cdot OH \rightarrow \cdot C(O)NH_2 + H_2O$$
  $$\cdot C(O)NH_2 + O2 \rightarrow HNCO + \cdot HO_2$$

  ----- Eq. 8 a and b

  Pathway 2:

  $$HCONH_2 + \cdot OH \rightarrow \cdot HC(O)NH + H_2O$$
  $$\cdot HC(O)NH + O2 \rightarrow HNCO + \cdot HO_2$$

  ----- Eq. 9 a and b

- From Acetamide : (Source: Barnes et al, 2010 [27])

  $$CH3CONH_2 + \cdot OH \rightarrow CH_3C(O) \cdot NH + H_2O$$
  $$CH_3C(O) \cdot NH \xrightarrow{CH_3\ Ejection} HNCO$$

  ----- Eq. 10 a and b

Isocyanic acid is formed photochemically from amides like formamide, acetamide, C3 amides and C4 amides reacting with the OH radical via pseudo first order reaction kinetics. The rates of formation of isocyanic acid can hence be calculated as given below:

$$(R_{HNCO})_{calculated} = [OH](k_{OH} \text{ x } [C])$$ ----- Eq. 11

Where:

[OH] = concentration of OH radical in the atmosphere (10.9×10^5 molecules/cm^3)

k_{OH} = rate constant of reaction of Formamide/Acetamide/C3 Amides/C4 Amides with OH radical

[C] = average concentration of Formamide/Acetamide/C3 Amides/C4 Amides from 06:00 am to 13:00pm

The concentration of OH radical in the atmosphere was taken as 10.9 x 10^5 molecules/cm^3 which is the global tropospheric average obtained from M Li, et al 2018[45].

The same equation is used for calculating the rate of formation of Isocyanic Acid from formamide, acetamide, C3 Amides and C4 amides by replacing the k_{OH} and [C] with the respective k_{OH} and [C] for each compound. The k_{OH} for each compounds were taken from the Figure 3.3 below obtained from Wang Z et al, 2020[25]. All these were added up to get a total calculated rate of formation.

Note that since there are multiple isomers for C3 and C4 amides, the highest and the lowest k_{OH} values for each were used so as to obtain an upper and lower bound for the calculated rate of formation from C3 and C4 amides respectively. The upper and lower bound rates of formation were then averaged to get an average calculated rate of formation from C3 and C4 amides respectively. The values obtained from formamide, acetamide, C3(upper and lower bound) and C4 amides(upper and lower bound) were then added to give the total calculated rate of formation of Isocyanic Acid (upper and lower bound). This was calculated for the period and the values are summarized in Table 5.

315 **S13. Production rates from different precursors of isocyanic acid**

316 **Table S3.** Production rates of precursors of isocyanic acid during the PRD campaign

Formula	Concentration[a] (ppbv)	Compound	k_{OH} (10^{-12} $cm^3 molecule^{-1} s^{-1}$)	Y_{HNCO}	Production rate (ppbv/h) Based on reported yield[b]	Production rate (ppbv/h) Assuming all N is converted to HNCO[c]
$CH(O)NH_2$	0.065 ± 0.016	Formamide	4.5 ± 0.4[5]	100%[5]	0.0031 ± 0.0016	0.0031 ± 0.0016
C_2H_5NO	0.029 ± 0.004	Acetamide	3.5 ± 1[26]	100%[26] ≤ 5%[27]	0.0011 ± 0.0006	0.0031 ± 0.0014
		N-methylformamide	10.1 ± 0.6[27]			
C_3H_7NO	0.18 ± 0.03	Propanamide	1.78 ± 0.43[27]	≤ 1%[29]	(1.6 ± 0.9)×10^{-4}	0.028 ± 0.013
		N-methylacetamide	5.42 ± 0.19[27]			
		N-ethylformamide	14.3[28]			
		N,N-dimethylformamide	8.5 ± 2.6[29]			
C_4H_9NO	0.012 ± 0.001	Butanamide	6.67[28]	≤ 1%[d]	(2.4 ± 1.1)×10^{-5}	0.0024 ± 0.0011
		N-methylpropanamide	7.6[27]			
		N,N-dimethylacetamide	19 ± 3[26, 27]			
		N-Ethylacetamide	9.59[28]			
		N-Propylformamide	17.5[28]			

Figure 3.3 The red box highlights the k_{OH} values used to calculate the rate of formation of Isocyanic Acid from various compounds (Source: Wang Z et al, 2020[25])

The total average R_{HNCO} Calculated for the period was 32.99 x 10^{-6} ppb/sec. As discussed in the previous section, since calculated rate of formation does not consider loss processes, it is expected to be greater than the observed rate of formation, which was observed in this case also. Hence the sink term was calculated by subtracting the observed rate of formation from the calculated rate of formation.

$$\boldsymbol{Sink\ Term} = (\boldsymbol{R_{HNCO}})_{\boldsymbol{calculated}} - (\boldsymbol{R_{HNCO}})_{\boldsymbol{observed}} \quad \text{----- Eq. 12}$$

3.3.3. Comparison between observed and calculated rates of formation of isocyanic acid and sink term

The Table 5 below summarizes all the observed and calculated rates of formation and sink terms for the period. The calculate rate of formation (32.99 x 10^{-6} ppb/sec) is ~ 3 times the observed rate of formation (10.7x10^{-6} ppb/sec). This leads to the average Sink term to be 22.29 x 10^{-6} ppb/sec. This again hints at the fact that there is a possible sink which is keeping the isocyanic acid concentrations lower than they would have been in absence of it. Some further analysis was done to try to determine the sink which is discussed in the next section.

	Rate of formation (ppb/sec)
R_{HNCO} observed (6:00-13:00 avg)	10.7×10^{-6}
R_{HNCO} calculated (upper bound)	35.57×10^{-6}
R_{HNCO} calculated (lower bound)	30.42×10^{-6}
R_{HNCO} calculated (average)	32.99×10^{-6}
Sink Term (upper bound)	24.87×10^{-6}
Sink Term (lower bound)	19.72×10^{-6}
Sink Term (average)	22.29×10^{-6}

Table 5. The values of Observed and Calculated Rates of Formation of Isocyanic Acid and Sink Term for the period

3.4 Assessing Deposition Sinks

Isocyanic acid has a lifetime of up to several decades against reaction with OH radicals in the atmosphere[33]. Also isocyanic acid is fairly stable against photolysis from solar radiation with a lifetime of several months against photolyis[34]. The major loss processes then comprise of heterogeneous losses in form of wet or dry deposition. Also a study found the pH of rainwater during the monsoon season in New Delhi and surrounding stations on an average was 6.39.[46] Apart from this other studies Panipat in Haryana also reported average pH of rainwater 5 to 6.86 and a study from Pune reported the average pH=6.6 of rainwater[47,48]. Thus pH can be assumed for our site in the range 6-7 and as discussed in section 1.4, at high pH (6-7), isocyanic acid has a very high solubility. Hence high humidity and rain events during monsoon could serve as a sink for uptake of isocyanic acid. In this section another possible sink of isocyanic acid was investigated – PM2.5. This was hypothesized because aerosol particles can provide with a surface for deposition.

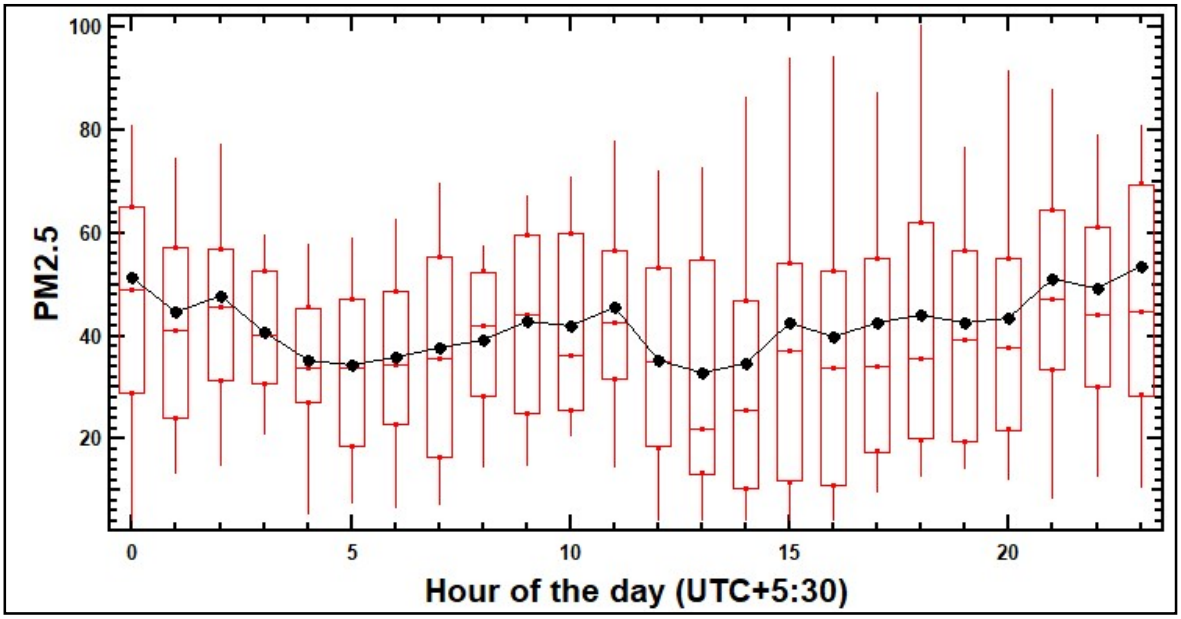

Figure 3.4 Diel profile for PM2.5 (µg/m^3) for the period

The diel profile of PM2.5 was plotted, as can be seen below in Figure 3.4. Further, an approximate surface area of PM2.5 available for deposition was calculated for using the average concentration from 18:00 pm to 23:00 pm (47.39 µg/m^3). This was done by assuming each particle to be a sphere, having a density of 1.5g/cm^3 and a diameter of 300nm. Further calculations were done as follows:

$$\textbf{\textit{Volume of 1 Particle of PM2.5}} = \frac{4}{3}\pi r^3 = 45\pi \text{ x } 10^{-22} \text{ m}^3 \quad \text{----- Eq. 13}$$

$$\textbf{\textit{Mass of 1 Particle of PM2.5}} = \textbf{\textit{Density}} \text{ x } \textbf{\textit{Volume}} = 45 \text{ x } 1.5 \text{ x } \pi \text{ x } 10^{-10}\mu g \quad \text{----- Eq. 14}$$

$$\textbf{\textit{No. of Particles of PM2.5 per m}}^3 \textbf{\textit{ of air}} = \frac{\textbf{\textit{Concentration}}}{45 \text{ x } 1.5 \text{ x } \pi \text{ x } 10^{-10}\mu g} \quad \text{----- Eq. 15}$$

$$\textbf{\textit{Available Surface Area of PM2.5 Particles per m}}^3 \textbf{\textit{ of air}} = 4\pi r^2 \text{ x } \textbf{\textit{Number of Particles of PM2.5 per m}}^3 \textbf{\textit{ of air}} \quad \text{----- Eq. 16}$$

	Calculations
PM 2.5 average conc. (avg 18:00-23:00)	47.39 µg/m^3
PM2.5 Upper bound (from 18:00-23:00)	53.41 µg/m^3
PM2.5 Lower bound (from 18:00-23:00)	42.71 µg/m^3
No. of PM 2.5 Particles (upper bound)	2.52 x 10^9 particles/m^3 of air
No. of PM 2.5 Particles (lower bound)	2.01 x 10^9 particles/m^3 of air
No. of PM 2.5 Particles (average)	2.23 x 10^9 particles/m^3 of air
Surface Area Available (upper bound)	7.13 x 10^{-4} m^2/m^3 of air
Surface Area Available (lower bound)	5.68 x 10^{-4} m^2/m^3 of air
Surface Area Available (average)	6.31 x 10^{-4} m^2/m^3 of air

Table 6. Available surface area of PM2.5 particles for nighttime (from 18:00 pm).

To calculate the deposition rates, night-time data (from 18:00 hrs) will be used since photochemical production at night is very little or negligible. Table 6 above summarizes the values obtained from the calculations for nighttime data. The equation for uptake coefficient and the rate of deposition was obtained from Tang M et al, 2010[49] as follows:

$$\frac{d[X]}{dt[X]} = k_{exp} = \frac{\gamma \cdot \bar{c}}{4} \cdot \frac{a}{V} \qquad \text{----- Eq. 17}$$

Where:

[X] = the gas-phase concentration of species X (molecule cm^{-3})

a/V = the surface area (a, cm2) per volume (V , cm^3)

$\bar{c}$ = the mean molecular velocity of the trace gas (cm s^{-1}) (~415 m/s)

γ = uptake coefficient

The k_{exp} was calculated using the fractional change in concentration of isocyanic acid from 18:00pm to 23:00 pm with value equal to 2.72 x 10^{-6} s^{-1}. The order of magnitude is same as the rates of formations and hence could mean that PM2.5 could be a contributing sink for isocyanic acid. The uptake coefficient was calculated to be 4.15 x 10^{-5}.

Also, the calculations were done for one rainy day in the season -14-07-2019. The average sink term for that day was 16.57 x 10^{-6} ppb/sec, the average k_{exp} was 6.06 x 10^{-6} s^{-1} and the uptake coefficient was calculated to be 2.9 x 10^{-4}. The sink term was lower than the seasonal average but the k_{exp} and the uptake coefiicient was greater than the seasonal average. This could be because the rain events might also contribute for the deposition of isocyanic acid.

Comparing this with the uptake coefficients for other gases in table 7 below, the uptake coefficient for isocyanic acid is less than that of NO_3, N_2O_5 and H_2O but greater than that of SO_2. In the study Tang et al 2010[49], the concentration of NO_3 dropped from ~450ppt to ~50ppt in presence of the ambient aerosols. From all this it can be hypothesized that while the uptake coefficient for isocyanic acid is less than that for NO_3, PM2.5 could still account for some of the deposition. Also since PM2.5 does not account for all the aerosols in the atmosphere and chemical, it can be said that the deposition rate and uptake coefficient calculated are underestimating the deposition of isocyanic acid on aerosols.

Gas	Uptake Coefficient
NO_3 [49]	9 x 10^{-3}
N_2O_5 [50]	1.3 x 10^{-2}
H_2O [51]	6.3 x 10^{-2}
SO_2 [52]	6.6 x 10^{-5}
HNO_3 [53]	3.3 x 10^{-2}
Acetic Acid(on Al_2O_3 in mineral dust) [54]	3 x 10^{-7}
HNCO (monsoon season average)	4.15 x 10^{-5}
HNCO (rainy day)	2.9 x 10^{-4}

Table 7. Uptake Coefficients for different gases and isocyanic acid

Chapter 4

Summary and Conclusion

- Isocyanic acid was only recently measured in the ambient air and not much is known about its atmospheric chemistry, sources and loss processes. It is an important trace VOC in the atmosphere as it may cause adverse effects on the climate, air quality and human health.
- The purpose of this study is to investigate the sources and sinks of ambient isocyanic acid concentrations at a suburban site in the NW-IGP. Isocyanic acid and its precursor compounds used in the analysis were quantified using an on-site PTR-MS with a 4-minute temporal resolution.
- The period to be studied was chosen as monsoon 2019 from 06-07-2019 to 08-08-2019 (n>12000). Average concentrations in ppb for the period were observed as 0.86, 5.4, 0.65, 0.23, and 0.13 for Isocyanic Acid, Formamide, Acetamide, Sum of C3 Amides and Sum of C4 amides respectively.
- The diel profiles for the period for Isocyanic Acid, Precursor compounds, Meteorological Parameters, CO and NOx were plotted.
- The BLH and the ventilation coefficient profiles were also plotted to account for the dilution effect during the daytime.
- Since all these compounds are formed photochemically, they had a daytime peak in concentration with peak isocyanic acid concentration being ~1 ppb.
- The observed and calculated rates of formation of isocyanic acid from precursor compounds were determined. It was found that the average calculated rate of formation for the period was 32.99 x 10^{-6} ppb/sec, ~3 times the observed rate of formation 10.7 x 10^{-6} ppb/sec.
- This is because calculated rate of formation just considers the source terms while observed rate also includes the sink terms. The average sink term was calculated to be 22.29 x 10^{-6} ppb/sec for the period.

- Since isocyanic acid is stable against photolysis and reaction with OH radical in the atmosphere, the main loss processes then include wet and dry deposition.
- Since aerosol particles provide a surface for deposition, it was hypothesized that PM2.5 particles could serve as potential sinks for deposition of isocyanic acid. Nighttime data was used to calculate the rate of deposition and uptake coefficient.
- The diel profile of PM2.5 was plotted for the period and the average concentration from 18:00 pm to 23:00 pm was 47.39 $\mu g/m^3$. Further the available surface area for deposition per m^3 of air was calculated.
- The rate of deposition and uptake coefficient was calculated as 2.72×10^{-6} s^{-1} and 4.15×10^{-5} respectively. This was comparable to uptake coefficients of some other gases and PM2.5 can be a potential contributor for the deposition of isocyanic acid.
- However it was beyond the scope of this study to prove it since not much is known about the deposition processes of isocyanic acid in the ambient air.
- Hence it is important that more studies be done on this compound, its sources and loss processes since concentrations exceeding 1ppb are thought to be concerning and potential causes of adverse health effects.

Bibliography

(1) Liebig, J.; Wöhler, F. Untersuchungen Über Die Cyansäure. *Ann. der Phys. und Chemie* **1830**, *96* (11). https://doi.org/10.1002/andp.18300961102.

(2) Roberts, J. M.; Veres, P. R.; Cochran, A. K.; Warneke, C.; Burling, I. R.; Yokelson, R. J.; Lerner, B.; Gilman, J. B.; Kuster, W. C.; Fall, R.; De Gouw, J. Isocyanic Acid in the Atmosphere and Its Possible Link to Smoke-Related Health Effects. *Proc. Natl. Acad. Sci. U. S. A.* **2011**. https://doi.org/10.1073/pnas.1103352108.

(3) Wang, Z.; Nicholls, S. J.; Rodriguez, E. R.; Kummu, O.; Hörkkö, S.; Barnard, J.; Reynolds, W. F.; Topol, E. J.; DiDonato, J. A.; Hazen, S. L. Protein Carbamylation Links Inflammation, Smoking, Uremia and Atherogenesis. *Nat. Med.* **2007**, *13* (10). https://doi.org/10.1038/nm1637.

(4) Beswick, H. T.; Harding, J. J. Conformational Changes Induced in Bovine Lens α-Crystallin by Carbamylation. Relevance to Cataract. *Biochem. J.* **1984**, *223* (1). https://doi.org/10.1042/bj2230221.

(5) Mydel, P.; Wang, Z.; Brisslert, M.; Hellvard, A.; Dahlberg, L. E.; Hazen, S. L.; Bokarewa, M. Carbamylation-Dependent Activation of T Cells: A Novel Mechanism in the Pathogenesis of Autoimmune Arthritis. *J. Immunol.* **2010**, *184* (12). https://doi.org/10.4049/jimmunol.1000075.

(6) Mishra, P.; Samarth, R.; Pathak, N.; Jain, S.; Banerjee, S.; Maudar, K. Bhopal Gas Tragedy: Review of Clinical and Experimental Findings after 25 Years. *Int. J. Occup. Med. Environ. Health* **2009**, *22* (3). https://doi.org/10.2478/v10001-009-0028-1.

(7) Gorisse, L.; Pietrement, C.; Vuiblet, V.; Schmelzer, C. E. H.; Köhler, M.; Duca, L.; Debelle, L.; Fornès, P.; Jaisson, S.; Gillery, P. Protein Carbamylation Is a

Hallmark of Aging. *Proc. Natl. Acad. Sci.* **2016**, *113* (5). https://doi.org/10.1073/pnas.1517096113.

(8) Plehiers, P. M. Comment on "Isocyanic Acid (HNCO) and Its Fate in the Atmosphere: A Review" by M. D. Leslie, M. Ridoli, J. G. Murphy and N. Borduas-Dedekind, *Environ. Sci.: Processes Impacts* , 2019, **21** , 793. *Environ. Sci. Process. Impacts* **2019**, *21* (12). https://doi.org/10.1039/C9EM00403C.

(9) Nilsson, L.; Lundquist, P.; Kågedal, B.; Larsson, R. Plasma Cyanate Concentrations in Chronic Renal Failure. *Clin. Chem.* **1996**, *42* (3). https://doi.org/10.1093/clinchem/42.3.482.

(10) Chandra, B. P.; Sinha, V. Contribution of Post-Harvest Agricultural Paddy Residue Fires in the N.W. Indo-Gangetic Plain to Ambient Carcinogenic Benzenoids, Toxic Isocyanic Acid and Carbon Monoxide. *Environ. Int.* **2016**, *88*, 187–197. https://doi.org/10.1016/j.envint.2015.12.025.

(11) Antonsen, S. G.; Bunkan, A. J. C.; Mikoviny, T.; Nielsen, C. J.; Stenstrøm, Y.; Wisthaler, A.; Zardin, E. Atmospheric Chemistry of Methyl Isocyanide–An Experimental and Theoretical Study. *J. Phys. Chem. A* **2020**, *124* (32). https://doi.org/10.1021/acs.jpca.0c05127.

(12) Hems, R. F.; Wang, C.; Collins, D. B.; Zhou, S.; Borduas-Dedekind, N.; Siegel, J. A.; Abbatt, J. P. D. Sources of Isocyanic Acid (HNCO) Indoors: A Focus on Cigarette Smoke. *Environ. Sci. Process. Impacts* **2019**, *21* (8), 1334–1341. https://doi.org/10.1039/c9em00107g.

(13) Wentzell, J. J. B.; Liggio, J.; Li, S.-M.; Vlasenko, A.; Staebler, R.; Lu, G.; Poitras, M.-J.; Chan, T.; Brook, J. R. Measurements of Gas Phase Acids in Diesel Exhaust: A Relevant Source of HNCO? *Environ. Sci. Technol.* **2013**, *47* (14). https://doi.org/10.1021/es401127j.

(14) Jathar, S. H.; Heppding, C.; Link, M. F.; Farmer, D. K.; Akherati, A.; Kleeman,

M. J.; de Gouw, J. A.; Veres, P. R.; Roberts, J. M. Investigating Diesel Engines as an Atmospheric Source of Isocyanic Acid in Urban Areas. *Atmos. Chem. Phys.* **2017**, *17* (14). https://doi.org/10.5194/acp-17-8959-2017.

(15) Brady, J. M.; Crisp, T. A.; Collier, S.; Kuwayama, T.; Forestieri, S. D.; Perraud, V.; Zhang, Q.; Kleeman, M. J.; Cappa, C. D.; Bertram, T. H. Real-Time Emission Factor Measurements of Isocyanic Acid from Light Duty Gasoline Vehicles. *Environ. Sci. Technol.* **2014**, *48* (19). https://doi.org/10.1021/es504354p.

(16) Wren, S. N.; Liggio, J.; Han, Y.; Hayden, K.; Lu, G.; Mihele, C. M.; Mittermeier, R. L.; Stroud, C.; Wentzell, J. J. B.; Brook, J. R. Elucidating Real-World Vehicle Emission Factors from Mobile Measurements over a Large Metropolitan Region: A Focus on Isocyanic Acid, Hydrogen Cyanide, and Black Carbon. *Atmos. Chem. Phys.* **2018**, *18* (23). https://doi.org/10.5194/acp-18-16979-2018.

(17) Liggio, J.; Stroud, C. A.; Wentzell, J. J. B.; Zhang, J.; Sommers, J.; Darlington, A.; Liu, P. S. K.; Moussa, S. G.; Leithead, A.; Hayden, K.; Mittermeier, R. L.; Staebler, R.; Wolde, M.; Li, S.-M. Quantifying the Primary Emissions and Photochemical Formation of Isocyanic Acid Downwind of Oil Sands Operations. *Environ. Sci. Technol.* **2017**, *51* (24). https://doi.org/10.1021/acs.est.7b04346.

(18) Sarkar, C.; Sinha, V.; Kumar, V.; Rupakheti, M.; Panday, A.; Mahata, K. S.; Rupakheti, D.; Kathayat, B.; Lawrence, M. G. Overview of VOC Emissions and Chemistry from PTR-TOF-MS Measurements during the SusKat-ABC Campaign: High Acetaldehyde, Isoprene and Isocyanic Acid in Wintertime Air of the Kathmandu Valley. *Atmos. Chem. Phys.* **2016**, *16* (6). https://doi.org/10.5194/acp-16-3979-2016.

(19) Zhao, R.; Lee, A. K. Y.; Wentzell, J. J. B.; Mcdonald, A. M.; Toom-Sauntry,

D.; Leaitch, W. R.; Modini, R. L.; Corrigan, A. L.; Russell, L. M.; Noone, K. J.; Schroder, J. C.; Bertram, A. K.; Hawkins, L. N.; Abbatt, J. P. D.; Liggio, J. Cloud Partitioning of Isocyanic Acid (HNCO) and Evidence of Secondary Source of HNCO in Ambient Air. *Geophys. Res. Lett.* **2014**, *41* (19). https://doi.org/10.1002/2014GL061112.

(20) Roberts, J. M.; Veres, P. R.; VandenBoer, T. C.; Warneke, C.; Graus, M.; Williams, E. J.; Lefer, B.; Brock, C. A.; Bahreini, R.; Öztürk, F.; Middlebrook, A. M.; Wagner, N. L.; Dubé, W. P.; de Gouw, J. A. New Insights into Atmospheric Sources and Sinks of Isocyanic Acid, HNCO, from Recent Urban and Regional Observations. *J. Geophys. Res. Atmos.* **2014**, *119* (2). https://doi.org/10.1002/2013JD019931.

(21) Mattila, J. M.; Brophy, P.; Kirkland, J.; Hall, S.; Ullmann, K.; Fischer, E. V.; Brown, S.; McDuffie, E.; Tevlin, A.; Farmer, D. K. Tropospheric Sources and Sinks of Gas-Phase Acids in the Colorado Front Range. *Atmos. Chem. Phys.* **2018**, *18* (16). https://doi.org/10.5194/acp-18-12315-2018.

(22) Woodward-Massey, R.; Taha, Y. M.; Moussa, S. G.; Osthoff, H. D. Comparison of Negative-Ion Proton-Transfer with Iodide Ion Chemical Ionization Mass Spectrometry for Quantification of Isocyanic Acid in Ambient Air. *Atmos. Environ.* **2014**, *98*. https://doi.org/10.1016/j.atmosenv.2014.09.014.

(23) Mungall, E. L.; Abbatt, J. P. D.; Wentzell, J. J. B.; Lee, A. K. Y.; Thomas, J. L.; Blais, M.; Gosselin, M.; Miller, L. A.; Papakyriakou, T.; Willis, M. D.; Liggio, J. Microlayer Source of Oxygenated Volatile Organic Compounds in the Summertime Marine Arctic Boundary Layer. *Proc. Natl. Acad. Sci.* **2017**, *114* (24). https://doi.org/10.1073/pnas.1620571114.

(24) Priestley, M.; Le Breton, M.; Bannan, T. J.; Leather, K. E.; Bacak, A.; Reyes-Villegas, E.; De Vocht, F.; Shallcross, B. M. A.; Brazier, T.; Anwar Khan, M.; Allan, J.; Shallcross, D. E.; Coe, H.; Percival, C. J. Observations of Isocyanate,

Amide, Nitrate, and Nitro Compounds From an Anthropogenic Biomass Burning Event Using a ToF-CIMS. *J. Geophys. Res. Atmos.* **2018**. https://doi.org/10.1002/2017JD027316.

(25) Wang, Z.; Yuan, B.; Ye, C.; Roberts, J.; Wisthaler, A.; Lin, Y.; Li, T.; Wu, C.; Peng, Y.; Wang, C.; Wang, S.; Yang, S.; Wang, B.; Qi, J.; Wang, C.; Song, W.; Hu, W.; Wang, X.; Xu, W.; Ma, N.; Kuang, Y.; Tao, J.; Zhang, Z.; Su, H.; Cheng, Y.; Wang, X.; Shao, M. High Concentrations of Atmospheric Isocyanic Acid (HNCO) Produced from Secondary Sources in China. *Environ. Sci. Technol.* **2020**. https://doi.org/10.1021/acs.est.0c02843.

(26) Leslie, M. D.; Ridoli, M.; Murphy, J. G.; Borduas-Dedekind, N. Isocyanic Acid (HNCO) and Its Fate in the Atmosphere: A Review. *Environ. Sci. Process. Impacts* **2019**, *21* (5), 793–808. https://doi.org/10.1039/c9em00003h.

(27) Barnes, I.; Solignac, G.; Mellouki, A.; Becker, K. H. Aspects of the Atmospheric Chemistry of Amides. *ChemPhysChem* **2010**, *11* (18). https://doi.org/10.1002/cphc.201000374.

(28) Borduas, N.; Murphy, J. G.; Wang, C.; da Silva, G.; Abbatt, J. P. D. Gas Phase Oxidation of Nicotine by OH Radicals: Kinetics, Mechanisms, and Formation of HNCO. *Environ. Sci. Technol. Lett.* **2016**, *3* (9). https://doi.org/10.1021/acs.estlett.6b00231.

(29) Lee, D.; Wexler, A. S. Atmospheric Amines – Part III: Photochemistry and Toxicity. *Atmos. Environ.* **2013**, *71*. https://doi.org/10.1016/j.atmosenv.2013.01.058.

(30) Bunkan, A. J. C.; Mikoviny, T.; Nielsen, C. J.; Wisthaler, A.; Zhu, L. Experimental and Theoretical Study of the OH-Initiated Photo-Oxidation of Formamide. *J. Phys. Chem. A* **2016**, *120* (8). https://doi.org/10.1021/acs.jpca.6b00032.

(31) Borduas, N.; da Silva, G.; Murphy, J. G.; Abbatt, J. P. D. Experimental and Theoretical Understanding of the Gas Phase Oxidation of Atmospheric Amides with OH Radicals: Kinetics, Products, and Mechanisms. *J. Phys. Chem. A* **2015**, *119* (19). https://doi.org/10.1021/jp503759f.

(32) Link, M. F.; Friedman, B.; Fulgham, R.; Brophy, P.; Galang, A.; Jathar, S. H.; Veres, P.; Roberts, J. M.; Farmer, D. K. Photochemical Processing of Diesel Fuel Emissions as a Large Secondary Source of Isocyanic Acid (HNCO). *Geophys. Res. Lett.* **2016**, *43* (8). https://doi.org/10.1002/2016GL068207.

(33) Tsang, W. Chemical Kinetic Data Base for Propellant Combustion. II. Reactions Involving CN, NCO, and HNCO. *J. Phys. Chem. Ref. Data* **1992**, *21* (4). https://doi.org/10.1063/1.555914.

(34) Brownsword, R. A.; Laurent, T.; Vatsa, R. K.; Volpp, H.-R.; Wolfrum, J. Photodissociation Dynamics of HNCO at 248 Nm. *Chem. Phys. Lett.* **1996**, *258* (1–2). https://doi.org/10.1016/0009-2614(96)00626-4.

(35) Borduas, N.; Place, B.; Wentworth, G. R.; Abbatt, J. P. D.; Murphy, J. G. Solubility and Reactivity of HNCO in Water: Insights into HNCO's Fate in the Atmosphere. *Atmos. Chem. Phys.* **2016**, *16* (2). https://doi.org/10.5194/acp-16-703-2016.

(36) Roberts, J. M.; Liu, Y. Solubility and Solution-Phase Chemistry of Isocyanic Acid, Methyl Isocyanate, and Cyanogen Halides. *Atmos. Chem. Phys.* **2019**, *19* (7). https://doi.org/10.5194/acp-19-4419-2019.

(37) Rosanka, S.; Vu, G. H. T.; Nguyen, H. M. T.; Pham, T. V.; Javed, U.; Taraborrelli, D.; Vereecken, L. Atmospheric Chemical Loss Processes of Isocyanic Acid (HNCO): A Combined Theoretical Kinetic and Global Modelling Study. *Atmos. Chem. Phys.* **2020**, *20* (11). https://doi.org/10.5194/acp-20-6671-2020.

(38) Young, P. J.; Emmons, L. K.; Roberts, J. M.; Lamarque, J.-F.; Wiedinmyer, C.; Veres, P.; VandenBoer, T. C. Isocyanic Acid in a Global Chemistry Transport Model: Tropospheric Distribution, Budget, and Identification of Regions with Potential Health Impacts. *J. Geophys. Res. Atmos.* **2012**, *117* (D10). https://doi.org/10.1029/2011JD017393.

(39) Sinha, V.; Kumar, V.; Sarkar, C. Chemical Composition of Pre-Monsoon Air in the Indo-Gangetic Plain Measured Using a New Air Quality Facility and PTR-MS: High Surface Ozone and Strong Influence of Biomass Burning. *Atmos. Chem. Phys.* **2014**, *14* (12). https://doi.org/10.5194/acp-14-5921-2014.

(40) Lindinger, W.; Jordan, A. Proton-Transfer-Reaction Mass Spectrometry (PTR–MS): On-Line Monitoring of Volatile Organic Compounds at Pptv Levels. *Chem. Soc. Rev.* **1998**, *27* (5). https://doi.org/10.1039/a827347z.

(41) de Gouw, J.; Warneke, C. Measurements of Volatile Organic Compounds in the Earth's Atmosphere Using Proton-transfer-reaction Mass Spectrometry. *Mass Spectrom. Rev.* **2007**, *26* (2). https://doi.org/10.1002/mas.20119.

(42) Sinha, V.; Custer, T. G.; Kluepfel, T.; Williams, J. The Effect of Relative Humidity on the Detection of Pyrrole by PTR-MS for OH Reactivity Measurements. *Int. J. Mass Spectrom.* **2009**, *282* (3). https://doi.org/10.1016/j.ijms.2009.02.019.

(43) Warneke, C.; Roberts, J. M.; Veres, P.; Gilman, J.; Kuster, W. C.; Burling, I.; Yokelson, R.; de Gouw, J. A. VOC Identification and Inter-Comparison from Laboratory Biomass Burning Using PTR-MS and PIT-MS. *Int. J. Mass Spectrom.* **2011**, *303* (1). https://doi.org/10.1016/j.ijms.2010.12.002.

(44) Kumar, V.; Chandra, B. P.; Sinha, V. Large Unexplained Suite of Chemically Reactive Compounds Present in Ambient Air Due to Biomass Fires. *Sci. Rep.* **2018**, *8* (1). https://doi.org/10.1038/s41598-017-19139-3.

(45) Li, M.; Karu, E.; Brenninkmeijer, C.; Fischer, H.; Lelieveld, J.; Williams, J. Tropospheric OH and Stratospheric OH and Cl Concentrations Determined from CH4, CH3Cl, and SF6 Measurements. *npj Clim. Atmos. Sci.* **2018**, *1* (1). https://doi.org/10.1038/s41612-018-0041-9.

(46) Tiwari, S.; Kulshrestha, U. C.; Padmanabhamurty, B. Monsoon Rain Chemistry and Source Apportionment Using Receptor Modeling in and around National Capital Region (NCR) of Delhi, India. *Atmos. Environ.* **2007**, *41* (27). https://doi.org/10.1016/j.atmosenv.2007.03.003.

(47) Momin, G. A. Study of Chemical Composition of Rainwater at an Urban (Pune) and a Rural (Sinhagad) Location in India. *J. Geophys. Res.* **2005**, *110* (D8). https://doi.org/10.1029/2004JD004789.

(48) Tiwari, Suresh & Srivastava, Manoj & Bisht, Deewan. (2008). Study of Chemical Composition of Rainwater for an Industrial City, Panipat in the State of Haryana.. Indian Journal of Radio & Space Physics. 37. 443-449. .

(49) Tang, M. J.; Thieser, J.; Schuster, G.; Crowley, J. N. Uptake of NO3 and N2O5 to Saharan Dust, Ambient Urban Aerosol and Soot: A Relative Rate Study. *Atmos. Chem. Phys.* **2010**, *10* (6). https://doi.org/10.5194/acp-10-2965-2010.

(50) Seisel, S.; Börensen, C.; Vogt, R.; Zellner, R. Kinetics and Mechanism of the Uptake of N2O5 on Mineral Dust at 298 K. *Atmos. Chem. Phys.* **2005**, *5* (12). https://doi.org/10.5194/acp-5-3423-2005.

(51) Seisel, S.; Pashkova, A.; Lian, Y.; Zellner, R. Water Uptake on Mineral Dust and Soot: A Fundamental View of the Hydrophilicity of Atmospheric Particles? *Faraday Discuss.* **2005**, *130*. https://doi.org/10.1039/b417449f.

(52) Adams, J. W.; Rodriguez, D.; Cox, R. A. The Uptake of SO2 on Saharan Dust: A Flow Tube Study. *Atmos. Chem. Phys.* **2005**, *5* (10). https://doi.org/10.5194/acp-5-2679-2005.

(53) Umann, B.; Arnold, F.; Schaal, C.; Hanke, M.; Uecker, J.; Aufmhoff, H.; Balkanski, Y.; Van Dingenen, R. Interaction of Mineral Dust with Gas Phase Nitric Acid and Sulfur Dioxide during the MINATROC II Field Campaign: First Estimate of the Uptake Coefficient γ_{HNO_3} from Atmospheric Data. *J. Geophys. Res.* **2005**, *110* (D22). https://doi.org/10.1029/2005JD005906.

(54) Tang, M.; Larish, W. A.; Fang, Y.; Gankanda, A.; Grassian, V. H. Heterogeneous Reactions of Acetic Acid with Oxide Surfaces: Effects of Mineralogy and Relative Humidity. *J. Phys. Chem. A* **2016**, *120* (28). https://doi.org/10.1021/acs.jpca.6b05395.